Inorganic Chemistry

Article

pubs.acs.org/IC

Oxidative Stretching of Metal−Metal Bonds to Their Limits

David W. Brogden,[†] Yevgeniya Turov,[†] Michael Nippe,[†] Giovanni Li Manni,[‡] Elizabeth A. Hillard,[§,∥] Rodolphe Clérac,[§,∥] Laura Gagliardi,[‡] and John F. Berry[†,*]

[†]Department of Chemistry, University of Wisconsin-Madison, 1101 University Avenue, Madison, Wisconsin 53706, United States

[‡]Department of Chemistry, Supercomputing Institute, and Chemical Theory Center, University of Minnesota, Minneapolis, Minnesota 55455, United States

[§]CNRS, CRPP, UPR 8641, F-33600 Pessac, France

[∥]Univ. Bordeaux, CRPP, UPR 8641, F-33600 Pessac, France

Supporting Information

ABSTRACT: Oxidation of quadruply bonded $Cr_2(dpa)_4$, $Mo_2(dpa)_4$, $MoW(dpa)_4$, and $W_2(dpa)_4$ (dpa = 2,2′-dipyridylamido) with 2 equiv of silver(I) triflate or ferrocenium triflate results in the formation of the two-electron-oxidized products $[Cr_2(dpa)_4]^{2+}$ (**1**), $[Mo_2(dpa)_4]^{2+}$ (**2**), $[MoW(dpa)_4]^{2+}$ (**3**), and $[W_2(dpa)_4]^{2+}$ (**4**). Additional two-electron oxidation and oxygen atom transfer by *m*-chloroperoxybenzoic acid results in the formation of the corresponding metal−oxo compounds $[Mo_2O(dpa)_4]^{2+}$ (**5**), $[WMoO(dpa)_4]^{2+}$ (**6**), and $[W_2O(dpa)_4]^{2+}$ (**7**), which feature an unusual linear M···M≡O structure. Crystallographic studies of the two-electron-oxidized products **2**, **3**, and **4**, which have the appropriate number of orbitals and electrons to form metal−metal triple bonds, show bond distances much longer (by >0.5 Å) than those in established triply bonded compounds, but these compounds are nonetheless diamagnetic. In contrast, the Cr−Cr bond is completely severed in **1**, and the resulting two isolated Cr^{3+} magnetic centers couple antiferromagnetically with J/k_B= −108(3) K [−75(2) cm^{-1}], as determined by modeling of the temperature dependence of the magnetic susceptibility. Density functional theory (DFT) and multiconfigurational methods (CASSCF/CASPT2) provide support for "stretched" and weak metal−metal triple bonds in **2**, **3**, and **4**. The metal−metal distances in the metal−oxo compounds **5**, **6**, and **7** are elongated beyond the single-bond covalent radii of the metal atoms. DFT and CASSCF/CASPT2 calculations suggest that the metal atoms have minimal interaction; the electronic structure of these complexes is used to rationalize their multielectron redox reactivity.

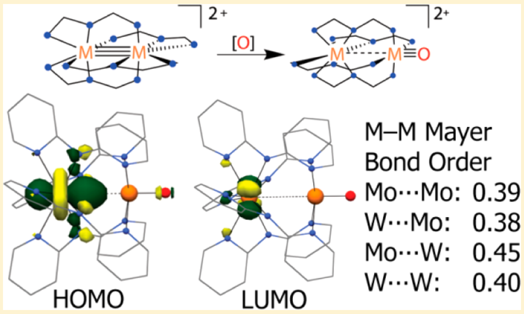

INTRODUCTION

The limits of metal−metal bonding are currently being tested in a number of ways. Since the discovery of stable quintuply bonded species,[1] the search for high metal−metal bond orders and supershort metal−metal distances has been quite fruitful.[2] Additionally, paramagnetic polymetallic clusters[3] and complexes with short heterometallic separations[4] are of renewed interest. At another frontier, uranium−uranium multiply bonded compounds remain tantalizing synthetic targets.[5] In this work, we tested another limit for metal−metal bonding: to see how far such a bond can be stretched before the bonding interactions are lost.

Bimetallic quadruply bonded paddlewheel compounds of chromium, molybdenum, and tungsten have been explored for several decades with a strong emphasis on their oxidation chemistry, which has been investigated primarily by electrochemical methods.[6] Several one- and two-electron-oxidized species have been isolated and characterized by crystallographic and spectroscopic methods.[7] Oxidation of the bimetallic unit leads to removal of metal−metal bonding electrons from the $\sigma^2\pi^4\delta^2$ quadruple-bond electron configuration, and the metal−metal distance is consequently elongated. This elongation approaches two distinct limiting cases: (1) Sequential oxidation can lead to small incremental increases of ca. 0.05 Å in the metal−metal bond length, consistent with removal of electrons from the metal−metal δ-bonding orbital to yield $[M_2]^{5+}$ species with a $\sigma^2\pi^4\delta^1$ configuration[7d−n,8] or triply bonded $[M_2]^{6+}$ complexes with a $\sigma^2\pi^4$ ground state.[7l−p,8,9] (2) Alternatively, oxidation can cause metal−metal bond scission, completely removing all metal−metal interactions.[7a,10] The quadruple bond between two Cr^{2+} ions can be severed not only by oxidation[10] but also by dissolution in certain solvents[11] because of the significantly weaker metal−metal orbital overlap in Cr_2 systems compared with Mo_2 and W_2 compounds and the inherently multiconfigurational nature of the Cr_2 unit: the $\sigma^2\pi^4\delta^2$ configuration can make up as little as 12% of the ground-state wave function for Cr_2^{4+} complexes.[12]

Herein are reported the synthesis and characterization of a systematic series of $[M_2]^{6+}$ (M_2 = CrCr, MoMo, MoW, and WW) species with bond distances between the two limiting cases described above. Computational methods were employed

Received: March 27, 2014
Published: April 21, 2014

© 2014 American Chemical Society dx.doi.org/10.1021/ic5007204 | *Inorg. Chem.* 2014, 53, 4777−4790

to support the experimental results and provide greater insight into the electronic structure of these complexes to determine the nature of their metal–metal interactions. Utilizing the 2,2′-dipyridylamido (dpa) equatorial ligand (Scheme 1) provides an additional N atom that does not coordinate in the $[M_2]^{4+}$ forms but can facilitate stretching of the metal–metal bonds in the two-electron-oxidized $[M_2]^{6+}$ species beyond the expected ca. 0.1 Å. Furthermore, we show that the stretched $[M_2]^{6+}$ complexes may be further oxidized by O atom donors to produce structurally novel $[M_2O]^{6+}$ species.[13] These oxo compounds feature a linear M···M≡O geometry in which the M···M distances are stretched outside the sum of their single-bond radii but are within the sum of their van der Waals radii. The relationship between the electronic structure and chemical reactivity of the oxo species is explored in this contribution.

Scheme 1. Oxidative Stretching of the Metal–Metal Bond Facilitated by the dpa Ligand

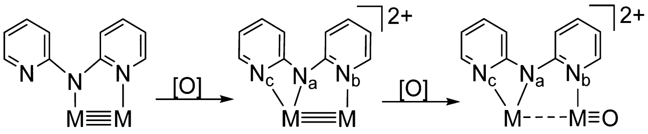

■ RESULTS AND DISCUSSION

Syntheses. The quadruply bonded starting materials for all of the complexes presented here, namely, $Cr_2(dpa)_4$,[4b] $Mo_2(dpa)_4$,[4d] $MoW(dpa)_4$,[4c] and $W_2(dpa)_4$,[8a] were all prepared as described elsewhere. Oxidation of $Cr_2(dpa)_4$ has to date only been studied electrochemically.[4f] The observed irreversible oxidation wave at −287 mV vs Fc/Fc^+ served as a poor prognostic for the prospect of isolating stable cationic $[Cr_2(dpa)_4]^{n+}$ compounds. Nevertheless, treatment of $Cr_2(dpa)_4$ with 2 equiv of silver triflate [Ag(OTf)] cleanly yielded the paramagnetic dication $[Cr_2(dpa)_4]^{2+}$ (**1**) as its triflate salt.

We recently reported one-electron oxidation of $Mo_2(dpa)_4$ and $W_2(dpa)_4$ to their corresponding monocations.[8a] In order to expand and complete this set of data, the heterometallic monocation $[MoW(dpa)_4]^+$ (**8**) was synthesized by oxidation of $MoW(dpa)_4$ with 1 equiv of Ag(OTf). Attempts to synthesize a monocationic chromium analogue $[Cr_2(dpa)_4]^+$ by one-electron oxidation of $Cr_2(dpa)_4$ were unsuccessful. The reaction with 1 equiv of oxidant produced the two-electron-oxidized product **1** in 50% yield with no signs that a one-electron-oxidized product was present (i.e., no comproportionation between $Cr_2(dpa)_4$ and $[Cr_2(dpa)_4]^{2+}$).

Electrochemical studies of the bimetallic compounds $[M_2(dpa)_4]^+$ displayed quasi-reversible oxidative waves, suggesting that the $[M_2(dpa)_4]^{2+}$ compounds could be isolated.[8a] Reaction of the neutral bimetallic starting materials $Mo_2(dpa)_4$, $MoW(dpa)_4$, and $W_2(dpa)_4$ with 2 equiv of oxidant at room temperature in dichloromethane resulted in the formation of the corresponding two-electron-oxidized products **2**, **3**, and **4** in reasonable yields (Scheme 2). Ag(OTf) was used as the oxidant for **3**; however, because of the lower solubility of **2** and **4** in dichloromethane, the more soluble ferrocenium triflate was found to be a better oxidant for these two complexes.[14]

Following the syntheses of the two-electron-oxidized products, new metal–oxo compounds akin to that reported[15] for ditungsten $[W_2O(dpa)_4]^{2+}$ (**7**), were prepared. The reactions of **2** and **3** with an oxidant capable of oxygen atom transfer such as *m*-chloroperoxybenzoic acid (*m*-CPBA) produced the desired dicationic bimetallic–oxo compounds **5** and **6**, respectively, in modest yields, as shown in Scheme 2. Attempts to synthesize the analogous dichromium–oxo compound were not successful. This observation may be attributed to the saturated coordination sphere of the pseudo-octahedral Cr^{3+} ions in **1**.

Scheme 2. Syntheses of Compounds 1–7

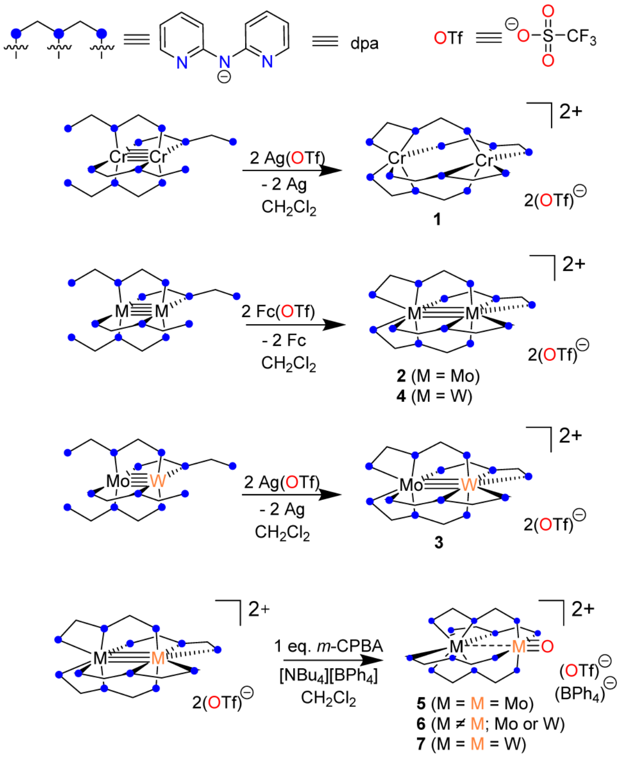

Crystal Structures. With the exception of **1** (which crystallizes in the space group $P2_1/c$ with $Z = 4$), the two-electron-oxidized compounds crystallize in the centrosymmetric space group $C2/c$, and the metal atoms of each complex ion lie along a crystallographic twofold rotation axis (Table 1). Thus, **2**–**4** all crystallize with one-half of the complex ion and one triflate counterion occupying the asymmetric unit of the structure. There are no solvent molecules in any of the asymmetric units for **1**–**4**. One triflate anion in the crystal structure of **1** is disordered. The bimetallic cores of **1**–**4** are surrounded by four dpa ligands in an expanded paddlewheel-type geometry (Figure 1 and Figure S1 in the Supporting Information). To accommodate the longer M–M separations in these compounds, the dpa ligands adopt a bridging/chelating coordination mode in which one pyridine N atom (N_b, the bridging nitrogen) binds to one metal atom and the other pyridine N atom (N_c, the chelating nitrogen) and the amido N atom (N_a) chelate to the other metal atom (Scheme 1). The metal–metal distance in **1**, 3.197(3) Å, is much longer than those in **2**–**4**, which decrease significantly with increasing tungsten content: 2.7981(2), 2.736(4), and 2.7156(3) Å for **2**, **3**, and **4**, respectively. Each metal atom is six-coordinate with respect to the bridging/chelating nitrogen atoms of the dpa ligand. The average $M-N_b$ and $M-N_c$ distances in **1**, 2.036[3] and 2.030[3] Å, respectively, are considerably shorter than the average $M-N_b$ distances of 2.144[1], 2.135[4], and 2.125[1] Å

Table 1. Crystallographic Data for **1**–**4** at 100 K

compound	**1**	**2**	**3**	**4**
formula	$Cr_2C_{40}H_{32}N_{12}(SO_3CF_3)_2$	$Mo_2C_{40}H_{32}N_{12}(SO_3CF_3)_2$	$MoWC_{40}H_{32}N_{12}(SO_3CF_3)_2$	$W_2C_{40}H_{32}N_{12}(SO_3CF_3)_2$
crystal system	monoclinic	monoclinic	monoclinic	monoclinic
space group	$P2_1/c$	$C2/c$	$C2/c$	$C2/c$
a (Å)	22.4721(5)	21.8793(6)	21.7812(9)	21.641(1)
b (Å)	8.8060(2)	12.7419(4)	12.7699(5)	12.797(6)
c (Å)	22.5134(5)	17.7890(5)	17.7974(7)	17.828(8)
α (deg)	90	90	90	90
β (deg)	108.192(1)	120.994(1)	120.937(3)	120.848(2)
γ (deg)	90	90	90	90
V (Å^3)	4251.3(2)	4251.2(2)	4246.0(3)	4238.8(3)
Z	4	4	4	4
ρ (Mg m^{-3})	1.692	1.829	1.969	2.110
$R_1{}^a$, $wR_2{}^b$ [$I > 2\sigma(I)$]	0.0406, 0.0938	0.0180, 0.0471	0.0313, 0.0711	0.0134, 0.0318
$R_1{}^a$, $wR_2{}^b$ (all data)	0.0626, 0.1048	0.0188, 0.0476	0.0461, 0.0773	0.0163, 0.0330

$^aR_1 = \sum||F_o| - |F_c||/\sum|F_o|$. $^bwR_2 = \{\sum[w(F_o^2 - F_c^2)^2]/\sum[w(F_o^2)^2]\}^{1/2}$, $w = 1/\sigma^2(F_o^2) + (aP)^2 + bP$, where $P = [\max(0 \text{ or } F_o^2) + 2(F_c^2)]/3$.

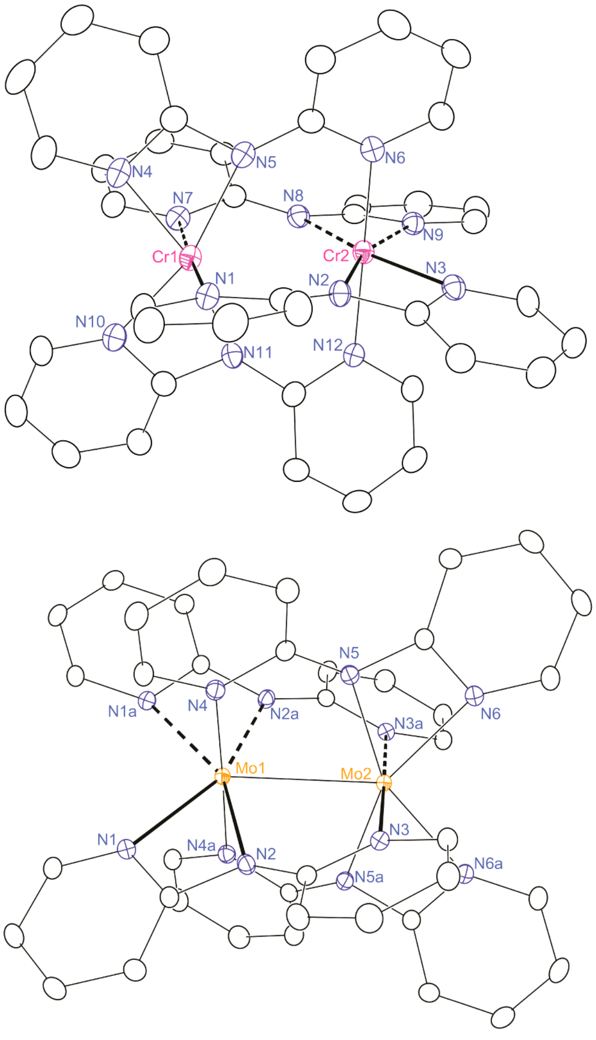

Figure 1. X-ray crystal structures of the dications in **1** (top) and **2** (bottom), with thermal ellipsoids drawn at the 50% probability level. Hydrogen atoms and counterions have been omitted for clarity.

in **2**, **3**, and **4**, respectively, and the average M–N$_c$ distances of 2.178[1], 2.192[4], and 2.194[1] Å in **2**, **3**, and **4**, respectively. This observation reflects the difference in the sizes of Cr and Mo/W. In contrast, the average M–N$_a$ distance in **1**, 2.116[3] Å, is only slightly less than the average M–N$_a$ distances of 2.163[1], 2.152[4], and 2.148[1] Å in **2**–**4**, respectively. Compounds **2**–**4** also display very different N$_b$–M–M–N$_c$ torsion angles (29.8°, 30.8°, and 31.3°, respectively) compared with the value in nearly eclipsed **1** (5.0°). The implications of this torsion with respect to the metal–metal bonding will be discussed below.

The oxo compounds **5**–**7** crystallize in the triclinic space group $P\overline{1}$, and the asymmetric unit in each case contains one dicationic $[M_2O(dpa)_4]^{2+}$ complex, one tetraphenylborate anion, and one triflate anion (the triflate anion in **6** is disordered with an approximately equal ratio of two orientations) as well as the inclusion of solvent in the crystal lattice (Table 2, Figure 2, and Figure S2 in the Supporting Information). In the heterometallic compound **6** there is metal ion disorder. In this disorder model, each metal ion site in the structure was modeled as being partially occupied by a Mo or W atom, with the Mo and W components constrained to have the same coordinates and thermal parameters.[16] It was therefore not possible to determine individual metal–metal or metal–oxo bond distances for the W⋯Mo≡O and Mo⋯W≡O heterometallic isomers. We observed different ratios of the W⋯Mo≡O and Mo⋯W≡O isomers in single crystals from different batches of **6**, varying from the W⋯Mo≡O isomer as the main component (89%) to the Mo⋯W≡O isomer as the major component (60%). Density functional theory (DFT) calculations predict the Mo⋯W≡O isomer to be slightly lower in energy (4.2 kJ/mol, 0.4 eV) than the W⋯Mo≡O isomer. This extremely small calculated energy difference between the two isomers provides support for the different observed single-crystal ratios of the Mo⋯W≡O and W⋯Mo≡O isomers. The metal–metal distances are elongated to 3.1251(2), 3.080(2), and 3.0735(3) Å in **5**–**7**, respectively, also decreasing as more W atoms are present in the molecule. It is interesting to note that the trend in metal–metal bond distances in **2**–**7** is opposite to what is observed in the quadruply bonded $M_2(dpa)_4$ compounds and their monocations, $[M_2(dpa)_4]^+$, in which the metal–metal distances increase with increasing number of tungsten atoms.[4c,8a] The metal–oxo distances are 1.662(1) Å in **5**, 1.702(2) Å in **6**, and 1.692(4) Å in **7**, consistent with a terminal, multiply bonded oxo group. In **5**–**7**, the metal atom bound to the oxo moiety is coordinated to four pyridine nitrogen atoms of the dpa ligands (M–N$_b$). The average M–N$_b$ distances in **5**–**7** are 2.156[2],

Table 2. Crystallographic Data for **5**−**8** at 100 K

compound	5	6	7	8
formula	$Mo_2C_{40}H_{32}N_{12}O(BC_{24}H_{20})(SO_3CF_3)\cdot C_4H_{10}O\cdot C_2H_3N$	$MoWC_{40}H_{32}N_{12}O(BC_{24}H_{20})(SO_3CF_3)\cdot C_4H_{10}O\cdot C_2H_3N$	$W_2C_{40}H_{32}N_{12}O(BC_{24}H_{20})(SO_3CF_3)\cdot C_4H_{10}O\cdot C_2H_3N$	$MoWC_{40}H_{32}N_{12}(SO_3CF_3)$
crystal system	triclinic	triclinic	triclinic	monoclinic
space group	$P\bar{1}$	$P\bar{1}$	$P\bar{1}$	$C2/c$
a (Å)	14.0730(4)	14.0889(5)	14.0857(6)	16.5234(8)
b (Å)	15.7381(5)	15.7173(5)	15.7157(6)	8.7975(5)
c (Å)	17.0039(5)	16.9811(6)	16.9784(7)	27.9784(1)
α (deg)	71.677(1)	71.584(2)	71.752(2)	90
β (deg)	69.779(1)	69.862(2)	69.914(2)	104.553(3)
γ (deg)	77.437(1)	77.420(2)	77.510(2)	90
V (Å^3)	3329.6(2)	3324.4(2)	3327.3(2)	3936.6(3)
Z	2	2	2	4
ρ (Mg m^{-3})	1.467	1.557	1.645	1.872
$R_1{}^a$, $wR_2{}^b$ [$I > 2\sigma(I)$]	0.0312, 0.0825	0.0279, 0.0799	0.0495, 0.1318	0.0390, 0.0837
$R_1{}^a$, $wR_2{}^b$ (all data)	0.0366, 0.0866	0.0333, 0.0828	0.0515, 0.1337	0.0604, 0.0916

$^aR_1 = \sum||F_o| - |F_c||/\sum|F_o|$. $^bwR_2 = \{\sum[w(F_o{}^2 - F_c{}^2)^2]/\sum[w(F_o{}^2)^2]\}^{1/2}$, $w = 1/\sigma^2(F_o{}^2) + (aP)^2 + bP$, where $P = [\max(0 \text{ or } F_o{}^2) + 2(F_c{}^2)]/3$.

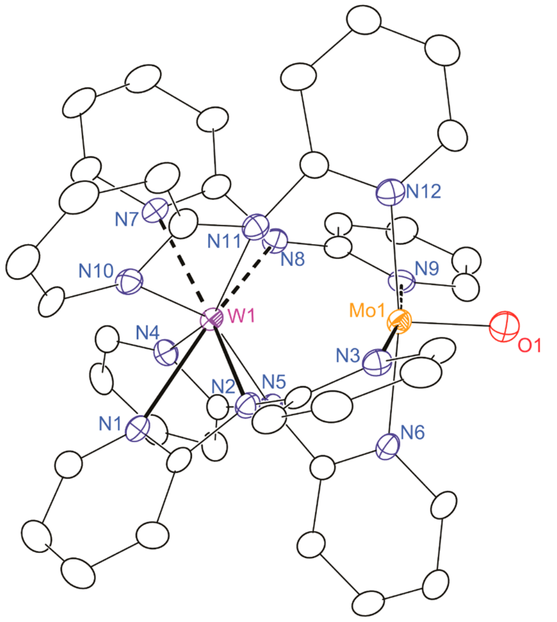

Figure 2. X-ray crystal structure of the dication in **6**, with thermal ellipsoids drawn at the 50% probability level. Only one orientation is shown for the disordered metal atoms. Hydrogen atoms, solvent molecules, and counterions have been omitted for clarity.

2.144[2], and 2.1385[4] Å, respectively. The other metal ion of the complex is eight-coordinate, with four metal−amide nitrogen bonds (M−N$_a$) and four metal−pyridine nitrogen bonds (M−N$_c$) in an approximate square-antiprismatic geometry. The average M−N$_a$ distances are 2.173[2], 2.170[2], and 2.175[4] Å and the average M−N$_c$ distances are 2.190[2], 2.197[2], and 2.201[4] Å for **5**−**7**, respectively. In **5**−**7** the average N$_b$−M−M−N$_c$ torsion angles are ca. 55° for each compound, and the metal−metal−oxygen angles are all very close to linear at ca. 178°, confirming the structural similarity of these compounds and allowing for the possibility of multicenter metal−metal−oxo bonding in these compounds.

Compound **8** crystallizes in the monoclinic space group $P2_1/c$ with one complex ion and one triflate counterion occupying the asymmetric unit. The metal atoms in **8** are positionally disordered as in **6**; thus, distinct Mo−N and W−N distances could not be differentiated. The bimetallic core is surrounded by four dpa ligands in an alternating paddlewheel geometry, and each metal ion is four-coordinate with respect to the chelating N atoms of dpa. One pyridine nitrogen atom of each dpa ligand is unbound to any metal atom (Figure 3). The Mo−W distance is 2.183(3) Å, which (as may be expected) falls between the reported metal−metal distances of $[Mo_2(dpa)_4]^+$ (2.14 Å) and $[W_2(dpa)_4]^+$ (2.22 Å).[8a] The average metal−nitrogen distance to the dangling pyridine (M···N$_{py}$) is 2.789[3] Å. The bound metal−nitrogen distances are much shorter, with average M−N$_{pyridine}$ (M−N$_{py}$) and M−N$_{amide}$ (M−N$_a$) distances of 2.155[3] and 2.116[3] Å, respectively. For the analogous $[Mo_2(dpa)_4]^+$ and $[W_2(dpa)_4]^+$ compounds, the direction angle of the unbound pyridine moiety, defined as the M−N$_a$−C−N$_{py}$ torsion angle,[17] was calculated to investigate the amount of electron donation from the pyridine nitrogen atom into the metal−metal π^* orbitals. The sum of the direction angles in **8** is 96.7[3]°, which is very similar to the values of 100.8[2]° and 100.5[3]° in $[Mo_2(dpa)_4]^+$ and $[W_2(dpa)_4]^+$, respectively. These large values for the direction angles indicate rather weak π^* interactions.

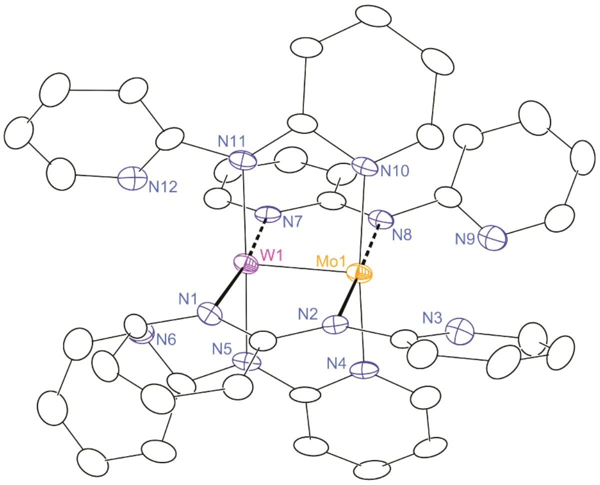

Figure 3. X-ray crystal structure for the monocation in **8**, with thermal ellipsoids drawn at the 50% probability level. Hydrogen atoms and the counterion have been omitted for clarity.

Electrochemistry. The redox properties of **8** are comparable to those of $[Mo_2(dpa)_4]^+$ and $[W_2(dpa)_4]^+$. Compound **8** has a reversible $[M_2(dpa)_4]^{0/+}$ redox couple at −0.94 V (all voltages versus Fc/Fc^+), which lies between that of $[Mo_2(dpa)_4]^+$ (−0.83 V) and $[W_2(dpa)_4]^+$ (−1.19 V).[8a] Like the ditungsten analogue, compound **8** experiences oxidations at −0.21 and 0.12 V, both of which appear to be quasi-reversible (Figure 4). Though $[W_2(dpa)_4]^+$ shows a well-defined third oxidation process,[8a] scans above 0.5 V for **8** yielded only ill-defined features.

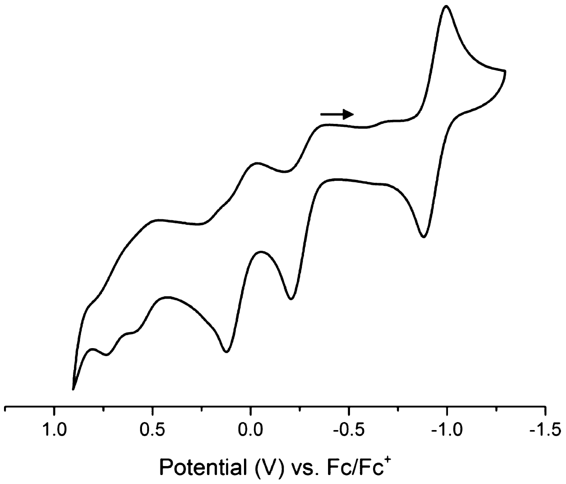

Figure 4. Cyclic voltammogram of **8** in CH_2Cl_2 with scan rate = 100 mV/s (0.1 M NBu_4PF_6).

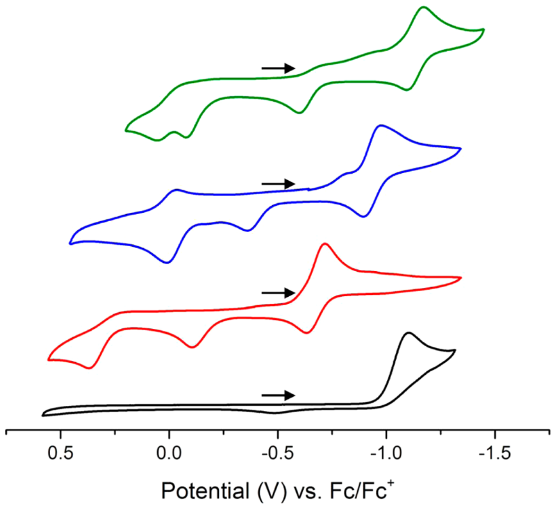

Figure 5. Cyclic voltammograms of **1** (black), **2** (red), **3** (blue), and **4** (green) in CH_3CN with scan rate = 100 mV/s (0.1 M NBu_4PF_6). Arrows indicate the scan direction.

Cyclic voltammograms were collected for **1**−**4** in acetonitrile (Figure 5 and Table 3). Compound **1** appears to be electrochemically fairly inert and displays only a single irreversible wave below −1 V. In cathodic scans, dicationic compounds **2**, **3**, and **4** display a single two-electron reductive wave to their corresponding neutral $M_2(dpa)_4$ compound followed in the reverse scan by two separate one-electron oxidative peaks to return to the $[M_2(dpa)_4]^{2+}$ state. The reversible waves attributed to the $[M_2(dpa)_4]^{0/+}$ redox couple thus occur at $E_{1/2}$ = −0.67, −0.93, and −1.13 V for **2**−**4**, respectively, assigned on the basis of the similarity to the $[M_2(dpa)_4]^{0/+}$ waves in the $[M_2(dpa)_4]^+$ compounds (vide supra). Compound **2** has two irreversible oxidative waves following the reversible $[M_2(dpa)_4]^{0/+}$ couple that occur at E_{a1} = −0.10 V and E_{a2} = 0.37 V. In compound **3**, however, there is an irreversible oxidative wave at E_{a1} = −0.36 V and a quasi-reversible wave at E_{a2} = −0.01 V. Compound **4** shows three irreversible oxidative waves following the reversible wave at E_{a1} = −0.59 V, E_{a2} = −0.07 V, and E_{a3} = 0.05 V.

To understand the reversibility and irreversibility of the features observed for **2**−**4**, it is pertinent to discuss the structural changes upon oxidation. Starting from the $M_2(dpa)_4$ compounds, the structural changes upon reversible oxidation to $[M_2(dpa)_4]^+$ compounds are minor, with an elongation of the metal−metal distances by ca. 0.05 Å and virtually no coordination of the dangling pyridine groups.[8a] The less reversible oxidation to $[M_2(dpa)_4]^{2+}$ occurs with a much larger change in the metal−metal distance, and now the dangling pyridine nitrogen atoms chelate to form six-coordinate metal centers as discussed in detail above. Further oxidation of the $[M_2(dpa)_4]^{2+}$ compounds would be suspected to sever the metal−metal bond and induce further structural changes that serve to render these additional voltammetric waves irreversible. Recording the scans at much lower or higher scan rates (25−300 mV/s) did not alter the reversibility of the observed waves, indicating that any nuclear rearrangements are either too slow or too fast to observe on the electrochemical time scale.

The cyclic voltammograms for **5**−**7** are shown in Figure 6. Compound **5** shows a reversible signal at $E_{1/2}$ = −1.03 V corresponding to the $[Mo_2O(dpa)_4]^{+/2+}$ redox couple. Following the reversible peak there is an irreversible reduction at E_c = −1.53 V. Compound **7** shows a reversible $[W_2O(dpa)_4]^{2+/3+}$ oxidative wave at $E_{1/2}$ = −0.02 V and an irreversible reduction at E_c = −1.48 V. The cyclic voltammogram of **6** shows features similar to those for **7**, displaying a reversible wave at $E_{1/2}$ = −0.01 V and an irreversible wave at E_c = −1.48 V. The signal at $E_{1/2}$ = −0.01 V is attributed to the oxidation of the W atom in the $W\cdots Mo{\equiv}O$ isomer (vide infra).[18]

Magnetic Measurements. The magnetic susceptibility (χ) of **1** was measured in an applied field of 1000 Oe between 1.8 and 340 K, and the data are shown in Figure 7 as a plot of χT versus T. The χT product at 340 K, estimated as 1.3 cm^3 K/mol, decreases rapidly until about 47 K, where the magnetic moment almost vanishes (χT = 0.02 cm^3 K/mol at 1.8 K). This thermal behavior and the observation that the high-temperature χT value is significantly lower than the expected Curie constant for two $S = {}^3/_2$ spin centers (3.75 cm^3 K/mol with g = 2) indicate the presence of strong antiferromagnetic coupling between the magnetic Cr^{III} centers. The magnitudes of the intracomplex magnetic interaction (J) and the Landé factor (g) were determined using the following Heisenberg spin Hamiltonian for a pair of isotropic $S = {}^3/_2$ spins: $\hat{H} = -2J\hat{\mathbf{S}}_1\cdot\hat{\mathbf{S}}_2$. In the framework of this model using the weak-field approximation ($g\mu_B H \ll k_B T$), an analytical expression for the magnetic susceptibility can be obtained applying the van Vleck equation:

$$\chi_{(\mathrm{Cr_2})} = \frac{2Ng^2\mu_B^{\ 2}}{k_BT}\,\frac{\exp(2x) + 5\exp(6x) + 14\exp(12x)}{1 + 3\exp(2x) + 5\exp(6x) + 7\exp(12x)}$$

where $x = J/k_BT$. As shown in Figure 7, the experimental data are well-fitted to this Heisenberg model over the whole range of

Table 3. Comparison of Electrochemical Data for $[M_2(dpa)_4]^{n+}$ Compounds (M_2 = Cr_2, Mo_2, MoW, W_2; n = 0, 1, 2)[a]

compound (solvent)	$[M_2(dpa)_4]^{0/+}$ $E_{1/2}$ (V)	$[M_2(dpa)_4]^{+/2+}$ E_{a1} (V)	$[M_2(dpa)_4]^{2+/3+}$ E_{a2} (V)	ref
$[Mo_2(dpa)_4]^+$ (CH_2Cl_2)	−0.83	−0.44	n.o.	8a
$[Mo_2(dpa)_4]^{2+}$ (CH_3CN)	−0.67	−0.10	0.37	this work
$[MoW(dpa)_4]$ (CH_2Cl_2)	−1.04	−0.33	n.o.	4c
$[MoW(dpa)_4]^+$ (CH_2Cl_2)	−0.94	−0.21	0.12	this work
$[MoW(dpa)_4]^{2+}$ (CH_3CN)	−0.93	−0.36	−0.01	this work
$[W_2(dpa)_4]^+$ (CH_2Cl_2)	−1.19	−0.57	n.o.	8a
$[W_2(dpa)_4]^{2+}$ (CH_3CN)	−1.13	−0.59	−0.07	this work

[a] All potentials are versus Fc/Fc$^+$; n.o. = not observed.

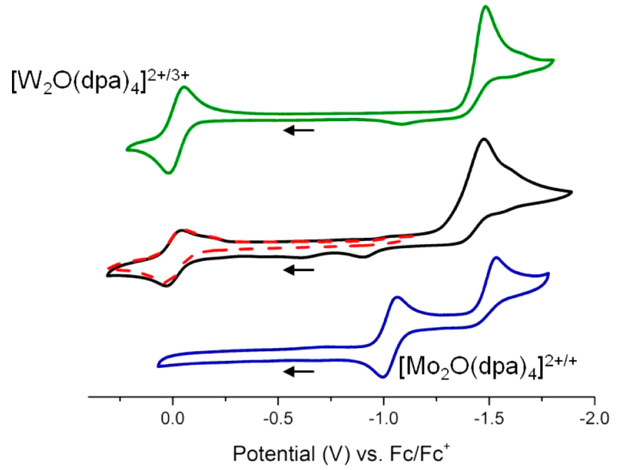

Figure 6. Cyclic voltammograms of **5** (blue), **6** (black and red), and **7** (green) in CH_3CN with scan rate = 50 mV/s (0.1 M NBu_4PF_6). Arrows indicate the scan direction.

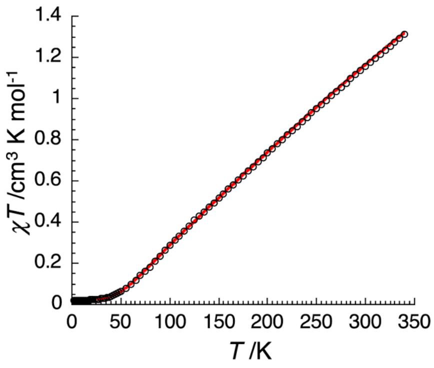

Figure 7. Temperature dependence of the χT product at 1000 Oe for **1** (with χ defined as the molar magnetic susceptibility, equal to M/H per mole of **1**); the red line is the fit using an isotropic Cr^{III} ($S_1 = S_2 = {}^3/_2$) dinuclear model.

temperatures, and the parameters were found to be g = 1.96(4) and J/k_B = −108(3) K [−75(2) cm^{-1}], taking into account a 1.3% $S = {}^3/_2$ paramagnetic Curie impurity. The observed J value is consistent with those of other dinuclear Cr^{III} complexes, which typically display J values of ca. −70 K (−50 cm^{-1}).[19]

Room-temperature X-band electron paramagnetic resonance (EPR) spectroscopy was used to probe the ground spin state of **8**. The compound displays an isotropic $S = {}^1/_2$ signal[20] (Figure S3 in the Supporting Information) with g_{iso} = 1.908. The A values associated with the observed splitting to the natural abundance of 14.31% for isotope ^{183}W ($I = {}^1/_2$) and the combined natural abundance of 25.47% for the isotopes ^{95}Mo and ^{97}Mo ($I = {}^5/_2$) are $A_{iso,Mo}$ = 80 MHz and $A_{iso,W}$ = 70 MHz. The fact that the magnitude of $A_{iso,Mo}$ is greater than that of the homometallic $[Mo_2(dpa)_4]^+$ compound and the magnitude of $A_{iso,W}$ is less than that of the homometallic $[W_2(dpa)_4]^+$ compound[8a] indicates that the unpaired electron in **8** resides in a δ orbital that is polarized toward Mo. The observed g value and polarization of the unpaired electron orbital to favor Mo for **8** are similar to those for the heterometallic carboxylate complex $[MoW(O_2C^tBu)_4]^+$, which showed g_{iso} = 1.881, $A_{iso,Mo}$ = 115.3 MHz, and $A_{iso,W}$ = 78.1 MHz.[7j]

NMR Spectroscopy. It was proposed earlier by our group that **4** possesses an unusually long triple bond because its ^1H NMR spectrum shows eight sharp resonances in the aromatic region corresponding to the eight dpa protons.[15] The ^1H NMR spectra of **2** and **3** also display eight sharp resonances in the aromatic region (Figure 8 and Figure S4 in the Supporting Information), indicating that the compounds are diamagnetic and that the molecular D_2 symmetry is preserved in solution. The ^1H NMR spectrum of compound **7**, reported earlier by our group,[15] features eight sharp resonances between 8.3−6.6 ppm, which were assigned to the eight dpa protons and the 20 protons corresponding to the tetraphenylborate counterion. The ^1H NMR spectra of **5** and **6** display similar aromatic features as **7**. Compound **5** has eight sharp resonances (Figure 8), whereas the spectrum of **6** displays better resolution, resulting in 10 distinct peaks corresponding to the eight dpa protons and the 20 tetraphenylborate protons (Figure 9).[21] The sharpness of the observed peaks and the anticipated

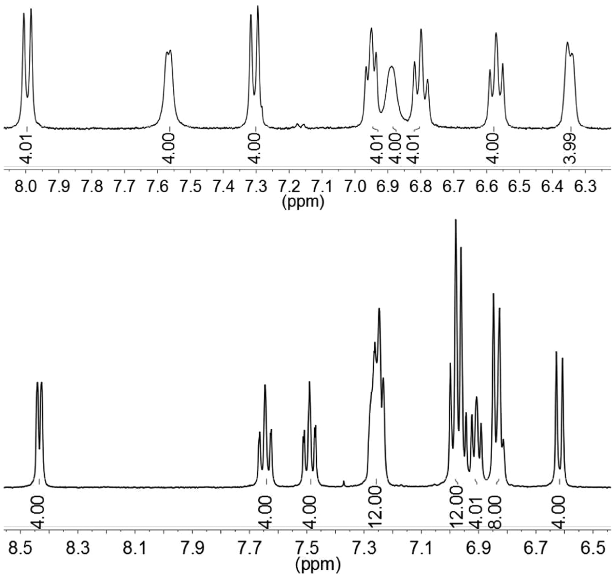

Figure 8. ^1H NMR spectra of (top) **2** and (bottom) **5** in CD_3CN at room temperature.

chemical shifts in the aromatic region indicate that compounds **5**−**7** are diamagnetic.

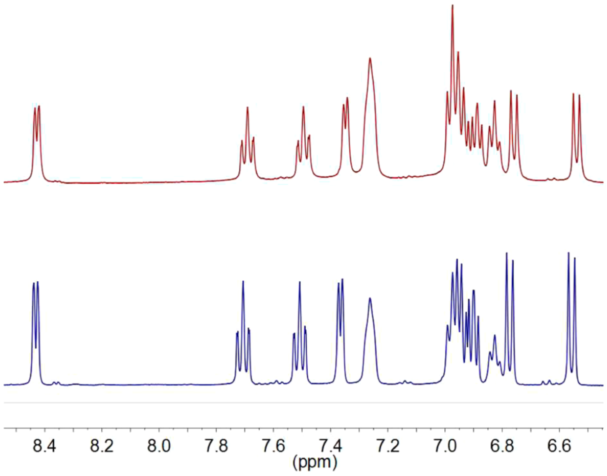

Figure 9. ^{1}H NMR spectra of **6** (top, red) and a 1:1 equimolar mixture of **3** and **6** (bottom, blue) in CD_3CN at room temperature.

Oxidative Stretching. Each of the starting bimetallic compounds $Cr_2(dpa)_4$, $Mo_2(dpa)_4$, $MoW(dpa)_4$, and $W_2(dpa)_4$ possesses a formal quadruple bond consisting of one σ bond, two π bonds, and one δ bond. Oxidation of these compounds by one electron removes one bonding δ electron, resulting in elongation of the metal−metal bond by 0.05 Å for $[Mo_2(dpa)_4]^+$ and $[MoW(dpa)_4]^+$ and 0.03 Å for $[W_2(dpa)_4]^+$.[8a] Further oxidation by a second electron would be expected to remove the other electron from the δ orbital and in turn yield another incremental increase in the metal−metal distance by ca. 0.05 Å. This is obviously not what happens in the present case, since the metal−metal bond elongation for **1**−**4** is on the order of $\Delta_A > 0.52$ Å, where Δ_A is defined as the difference between the metal−metal bond distances in the neutral bimetallic compound and its corresponding two-electron-oxidized compound. We likewise define Δ_B as the difference between the metal−metal bond distances in the $[M_2(dpa)_4]^{2+}$ dication and its corresponding $[M_2O(dpa)_4]^{2+}$ metal−oxo compound (Table 4). The large Δ_A value for **1** (1.25 Å) and the observed paramagnetic behavior upon two-electron oxidation are indicative of full cleavage of the metal−metal bond. For **2**−**4**, the bond elongation is significantly less (0.52 Å < Δ_A < 0.70 Å), representing a "stretching" of the metal−metal bond.

Two-electron oxidation of **2**−**4** and oxygen atom transfer by *m*-CPBA results in the formation of the novel bimetallic metal−oxo compounds **5**−**7**. The metal−metal bond is further elongated in **5**−**7** by 0.32 Å < Δ_B < 0.35 Å. The values of Δ_B are significantly less than the values of Δ_A, suggesting that the metal−metal bonds are now "stretched" to their limit. It is fitting to consider the single-bond covalent radii[22] as well as the van der Waals radii[23] of the metals in **1**−**7** to determine whether a metal−metal interaction should be considered. The sums of the single-bond radii are 2.76 Å for two Mo atoms, 2.75 Å for a Mo atom and a W atom, and 2.74 Å for two W atoms. [22] The corresponding van der Waals sums are 4.90, 5.02, and 5.14 Å, respectively. [23] The metal−metal distances in **3** and **4** are thus within the sum of the van der Waals radii but at the limit of what may be considered a single bond. The metal−metal distances in **5**−**7** are >0.4 Å longer than the single-bond radii but still within the van der Waals radii, suggesting that, to a first approximation, there is only weak metal−metal bonding in **5**−**7**. A further piece of supporting evidence for weak metal−metal interactions here is the decreasing metal−metal distances observed upon going from Mo_2 to MoW to W_2 in **2**−**7**. Presumably, this effect must be a consequence of improved orbital overlap between W atoms, resulting in a small but nonzero metal−metal interaction. This issue, inter alia, was investigated by computational methods as described below.

Density Functional Theory Calculations. DFT methods were employed to characterize the ground-state electronic structures and investigate the metal−metal interactions in **1**−**7**. The optimized geometric parameters are presented in Table 4. The calculated metal−metal bond distances for **1** and **2** are slightly overestimated by DFT (3.229 and 2.840 Å, respectively), and the calculated metal−metal bond distances for **3** and **4** are slightly underestimated by DFT (2.678 and 2.677 Å, respectively). For **5**−**7**,[24] DFT slightly overestimates the metal−metal distances at 3.161, 3.117, and 3.108 Å, respectively, but the calculations capture the trend of shorter metal−metal separations in going from **5** to **6** to **7**. The calculated metal−oxo distances of 1.672, 1.697, and 1.704 Å for **5**−**7**, respectively, agree well with the experimental values. All

Table 4. Selected Bond Distances and Angles in 1−8

compound	M−M (Å)	M−O (Å)	M−N_a, av (Å)	M−N_b, av (Å)	M−N_c, av (Å)	M−N_{py}, av (Å)	M···N_{py}, av (Å)	N_b−M−M−N_c, av (deg)	Δ_A (Å)	Δ_B (Å)
1	3.197(3)		2.116[3]	2.036[3]	2.030[3]			5.05	1.254	
1 DFT	3.229		2.132	2.159	2.049			4.8	1.432	
2	2.7981(2)		2.163[1]	2.144[1]	2.178[1]			29.87	0.701	
2 DFT	2.840		2.177	2.167	2.193			27.2	0.743	
3	2.736(4)		2.152[4]	2.135[4]	2.192[4]			30.80	0.601	
3 DFT	2.678		2.154	2.144	2.213			32.5	0.524	
4	2.7156(2)		2.148[1]	2.125[1]	2.194[1]			31.36	0.522	
4 DFT	2.677		2.147	2.139	2.213			33.3	0.481	
5	3.1251(2)	1.662(1)	2.173[2]	2.156[2]	2.190[2]			55.86		0.327
5 DFT	3.161	1.672	2.202	2.165	2.219			56.6		0.321
6	3.080(2)	1.702(2)	2.170[2]	2.144[2]	2.197[2]			55.59		0.344
6 DFT	3.117	1.697	2.189	2.144	2.221			56.5		0.439
7	3.0735(3)	1.692(4)	2.175[4]	2.138[4]	2.201[4]			55.77		0.357
7 DFT	3.108	1.704	2.189	2.145	2.225			55.9		0.431
8	2.183(3)		2.116[3]			2.155[3]	2.789[3]			

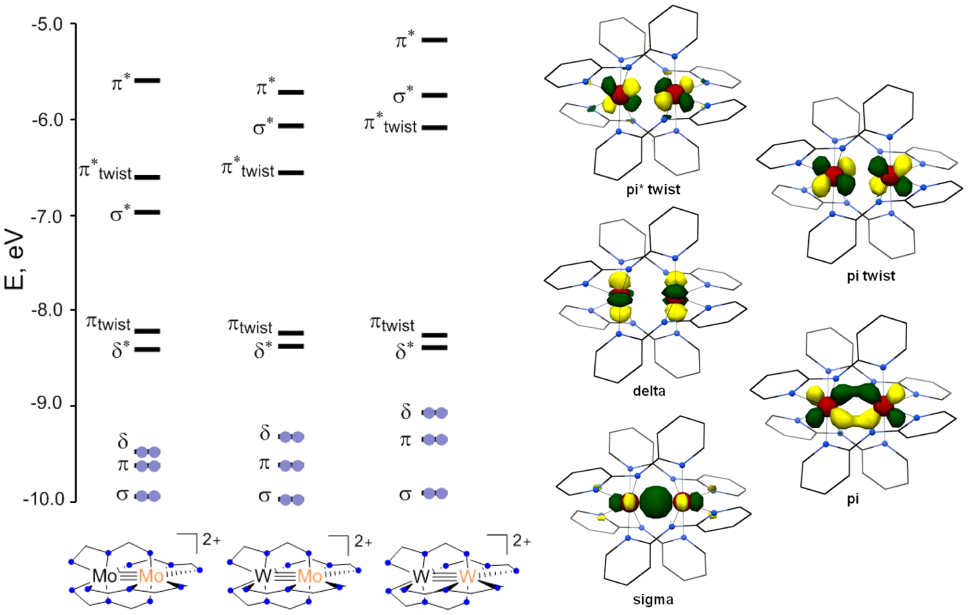

Figure 10. Calculated molecular orbital diagrams for $[M_2(dpa)_4]^{2+}$ compounds (left). Representative molecular orbitals for $[W_2(dpa)_4]^{2+}$ (right).

of the metal−nitrogen distances and N_b−M−M−N_c torsion angles are well-reproduced by DFT. While the calculated Δ_A value for **1** is slightly larger (by ca. 0.2 Å) than the experimental value, those for **2**, **3**, and **4** correspond well to the crystal structure values. The calculated Δ_B value for **5** reproduces the experimental value very well, and the calculated Δ_B values for **6** and **7** are slightly overestimated by ca. 0.1 Å.

The electronic ground state for neutral $M_2(dpa)_4$ compounds is $\pi^4\sigma^2\delta^2$. The π-type orbitals are lower in energy than the σ-type orbitals as a result of strong antibonding interactions between the M_2 σ orbital and the N atoms' lone pairs that raise the σ orbital above the π level.[25] Oxidation by two electrons would be expected to result in removal of the δ-bonding electrons and a $\pi^4\sigma^2$ electron configuration, composed of a σ bond and two π bonds. The computational results show that this is not the case, and instead, a rather unique electronic ground state of $\sigma^2\pi^2\delta^2$ is observed for the $[M_2(dpa)_4]^{2+}$ compounds (Figure 10). The binding of the extra pyridine groups and the twisting of the dpa ligands around the metal−metal core that results in torsion angles of ca. 30° cause a change in the molecular orbital ordering. The new molecular orbital diagram is made up of σ, π, and δ orbitals as well as very distorted empty π orbitals, which are labeled as π_{twist}. The distortion of the π_{twist} orbitals that stems from the N_b−M−M−N_c torsion in the dpa ligands forces them to be higher in energy than the δ and δ* orbitals. As expected from the trend in the metal−metal bond distances, the calculated Mayer bond order (MBO) increases from 1.03 to 1.32 to 1.72 for **2**−**4**, respectively, but remains notably less than an idealized triple-bond value of 3.0. The trend in increasing metal−metal bond strength in going from **2** to **4** can also be observed by the increasing energy difference between the σ and σ* orbitals. In **2**, the σ* orbital is lower in energy than the π^*_{twist} orbital; however, in **3** and **4** the σ* orbital is higher in energy than the π^*_{twist} orbital. Compound **4** displays the largest energy gap between the σ and σ* orbitals, 4.2 eV, which correlates with the shortest metal−metal distance and strongest metal−metal bond. Combining the molecular orbital picture with the MBO analysis, DFT indicates that there is indeed a bond between the metal atoms in the $[M_2(dpa)_4]^{2+}$ compounds. We classify the bond as having a strong σ interaction with weak overlap of the π and δ orbitals, which leads to the partial triple-bond character and observed diamagnetism of the compounds.

We note a similarity between the $\sigma^2\pi^2\delta^2$ molecular orbital splitting predicted for **2**−**4** and that in edge-shared bioctahedral systems of group 6 metals.[26] Such compounds have metal−metal bond distances similar to those in the compounds reported here.[26] Broken-symmetry calculations performed on the parent $[M_2Cl_{10}]$ complexes (M = Cr, Mo, W)[27] predict, at the fully delocalized limit, coupling between the two metal ions that results in metal−metal bonding/antibonding combinations of σ, π, and δ symmetry. Therefore, the molecular orbital splitting for $[M_2Cl_{10}]^{4-}$ compounds is also $\sigma < \pi < \delta < \delta^* < \pi^* < \sigma^*$, with the σ, π, and δ orbitals doubly occupied. This splitting pattern is similar to that seen in the molecular orbital diagrams predicted for the $[M_2(dpa)_4]^{2+}$ compounds; however, in the $[M_2(dpa)_4]^{2+}$ compounds, there is one more metal−metal-based orbital, which leads to the predicted π_{twist} and π^*_{twist} orbitals. Addition of an electron pair to the π_{twist} orbital can result in re-reduction of **2**−**4** to the quadruply bonded starting complexes. Such rereduction of an edge-sharing bioctahedral complex to reform the quadruple bond is, to our knowledge, not known.

In contrast to **2**−**4**, the Cr atoms in dication **1** were calculated to be noninteracting and to behave as individual six-coordinate Cr^{3+} ions. The electronic structure of **1** was modeled using the broken-symmetry formalism[28] to evaluate the magnitude of the spin coupling between the two Cr^{III} centers. As expected, each Cr^{III} ion possesses a set of singly occupied t_{2g}-like orbitals (Figure 11), which are predicted to couple with a coupling constant of $J = -75\ cm^{-1}$,[29] which matches the experimental value exactly (vide supra).

DFT was also used to study the potential metal−metal interactions in **5**−**7**, in which the metal−metal distances lay outside the single-bond covalent radii of the corresponding metal atoms. The results show that, to a first approximation, the two M^{4+} ions may be treated as independent of each other. Thus, the eight-coordinate metal center can be considered to be

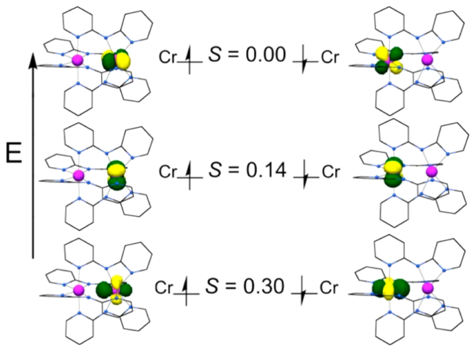

Figure 11. Broken-symmetry molecular orbital diagram for $[Cr_2(dpa)_4]^{2+}$ with the corresponding molecular orbitals shown to the right and left. The *S* values indicate the calculated overlap between corresponding orbitals.

in an approximate square-antiprismatic geometry with a $d_{z^2} < d_{x^2-y^2}, d_{xy} < d_{xz}, d_{yz}$ metal orbital splitting, and the second metal center should display the characteristic tetragonal metal–ligand multiple-bond orbital splitting (i.e., $d_{xy} < d_{xz}, d_{yz} < d_{x^2-y^2} < d_{z^2}$).[30] This is indeed the case, as displayed in Figure 12. Both metal atoms have a d^2 configuration, with one electron pair that fills the expected molecular orbital for each of the two metal atoms, namely, $(d_{z^2})^2$ for the eight-coordinate metal atom and $(d_{xy})^2$ for the five-coordinate metal atom. The only hint of delocalization along the $M_A\cdots M_B{\equiv}O$ chain is the fact that the filled d_{z^2} orbital of the eight-coordinate metal center has a small but significant amount of oxygen atom character (1.6%, 1.8%, and 2.8% for **5**, **6**, and **7**, respectively) from the terminal oxo group, which increases with the tungsten content of the molecules. This oxygen character may indicate a small amount of $M_A\cdots O$ "long bond" character typical of three-center/four-electron bonds.[31] DFT also confirms the presence of a metal–oxygen triple bond consisting of a σ bond and two π bonds ($\sigma^2\pi^4$), which are much lower in energy than the frontier orbitals shown in Figure 12. The calculated MBOs for the metal–oxygen bond are 2.27, 2.31, and 2.31 for **5**, **6**, and **7**, respectively. The metal–metal MBOs for **5**–**7** are all ca. 0.4, which are less than for a single bond but, notably, nonzero.

CASSCF/CASPT2 Calculations. Metal–metal bonds can be multiconfigurational in nature, and thus, the complete-active-space self-consistent field (CASSCF) method should provide a more accurate picture of the ground-state wave functions of these compounds. CASSCF followed by second-order perturbation theory (CASPT2) calculations were performed on **2**–**7**. For **2**–**4**, the singlet spin state was found to be the ground state and indeed shows strong multiconfigurational character with several competing configurations. The dominant configuration is $\sigma^2\pi^2\delta^2$, as suggested from the DFT results (vide supra), with a weight of 24% for **2**, 33% for **3**, and 42% for **4** (Table 5). Other relevant configurations are mainly double excitations from the bonding to the antibonding active orbitals. Analysis of the metal–metal effective bond orders (EBOs) for **2**–**4** shows an increase in the bond order with increasing W character (1.01 for **2**, 1.33 for **3**, and 1.59 for **4**), as anticipated from the increased contribution of the triply bonded configuration to the ground state. This result nicely explains the increase in metal–metal bond strength as additional W atoms are included in the compounds. The active-space molecular orbitals are shown in Figure 13.

Table 5. CASSCF/CASPT2-Calculated Electron Configurations for 2–4[a]

$[Mo_2(dpa)_4]^{2+}$	$[MoW(dpa)_4]^{2+}$	$[W_2(dpa)_4]^{2+}$
24% $\sigma^2\pi^2\delta^2$	33% $\sigma^2\pi^2\delta^2$	42% $\sigma^2\pi^2\delta^2$
16% $\sigma^2\pi^2\delta^{*2}$	17% $\sigma^2\pi^2\delta^{*2}$	18% $\sigma^2\pi^2\delta^{*2}$
14% $\sigma^2\pi^d\delta^u\delta^{*d}\pi^{*u}$	14% $\sigma^2\pi^d\delta^u\delta^{*d}\pi^{*u}$	12% $\sigma^2\pi^d\delta^u\delta^{*d}\pi^{*u}$
13% $\sigma^2\pi^2\pi^{*2}$	12% $\sigma^2\pi^2\pi^{*2}$	11% $\sigma^2\pi^2\pi^{*2}$

[a] A superscript "u" denotes a spin-up electron, and a superscript "d" denotes a spin-down electron.

CASSCF/CASPT2 calculations on **5**–**7** show the singlet spin state to be the lowest in energy and dominated by a metal–oxo $\sigma^2\pi^4$ configuration (93% for **5** and **6** and 94% for **7**), corresponding to metal–oxygen EBOs of 2.86, 2.86, and 2.85 for **5**, **6**, and **7**, respectively. The other occupied orbitals are a d_{xy} orbital localized on the oxygen-bound metal atom and a d_{z^2} orbital localized on the eight-coordinate metal atom (Figure S5 in the Supporting Information). Since the active-space

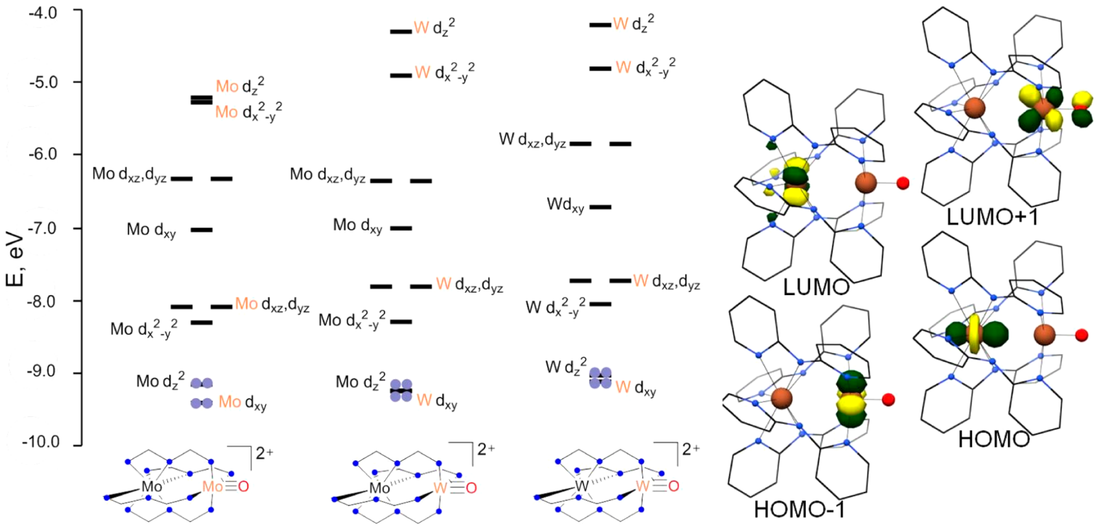

Figure 12. Molecular orbital diagrams for $[M_2O(dpa)_4]^{2+}$ compounds based on the results of DFT calculations (left). Representative molecular orbitals for $[Mo_2O(dpa)_4]^{2+}$ (right).

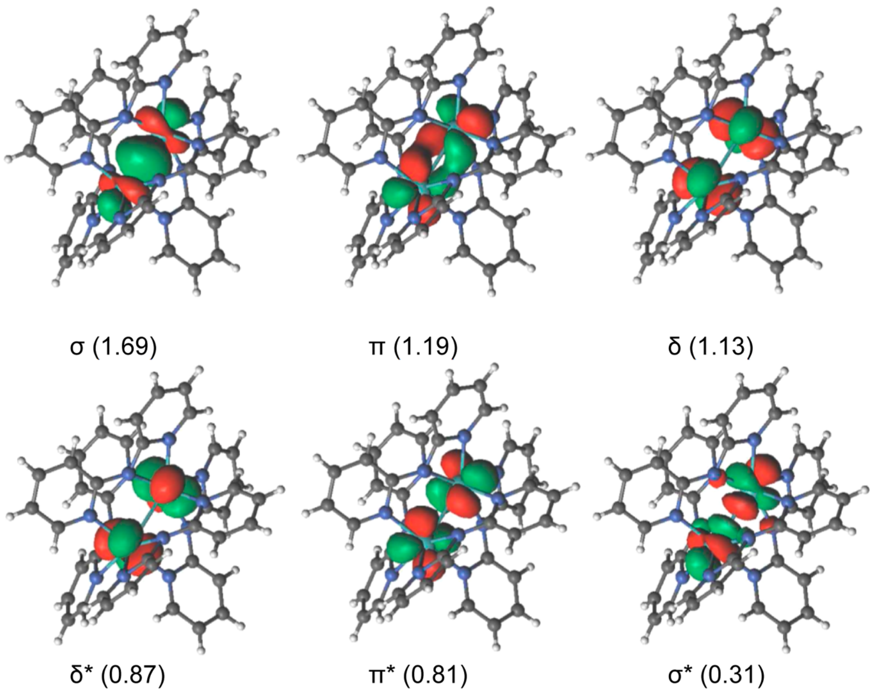

Figure 13. Active-space molecular orbitals for the CAS(6,6) calculation on **2**. The occupation number for each orbital is given in parentheses.

molecular orbitals are localized on each metal atom, no partial metal−metal interactions can be seen from the CASSCF data.

Oxygen Atom Transfer Reactivity. To further probe the properties of **5**−**7** in solution with respect to the possibility of oxygen atom transfer, 1:1 equimolar mixtures of **2** and **5**, **4** and **7**, **2** and **7**, and **4** and **5** were investigated by ^{1}H NMR spectroscopy. In each case, the mixture showed two unique sets of ^{1}H NMR signals corresponding to the two compounds in solution (Figures S6−S9 in the Supporting Information).These results indicate that the homometallic M···M≡O compounds do not perform intermolecular oxygen atom transfer to the $[M_2(dpa)]^{2+}$ species on the NMR time scale. However, the NMR spectrum of a 1:1 equimolar mixture of the heterometallic compounds **3** and **6** displays only one set of dpa resonances (Figure 9) with chemical shifts that fall between the shifts of **3** and **6** by themselves, as shown in the stacked NMR plot (Figure 14). A low-temperature ^{1}H NMR study (−35 °C in acetonitrile) was performed on the equimolar 1:1 mixture of **3** and **6**, but no separation or broadening of the dpa resonances was observed. Thus, unlike the homometallic compounds, it appears as though **3** and **6** are able to undergo oxygen atom transfer with one another. We note, however, that **6** does not perform oxygen atom transfer with triphenylphosphine. On the other hand, we previously reported the surprising reactivity of **7** with the more reducing tri-*tert*-butylphosphine and tri-*n*-butylphosphine.[15] As discussed further in the next section, these reactions are not oxygen atom transfer reactions.

Relating Electronic Structure to Reactivity. The calculated electronic structure of the M···M≡O species provides a useful framework for understanding the unusual reactivity of **7**.[15] We found that **7** reacts with trialkylphosphines via one-electron oxidation of the phosphine, giving rise to a highly reactive phosphinyl radical intermediate species (Scheme 3), instead of the expected reaction via oxygen atom transfer to yield phosphine oxide.[15]

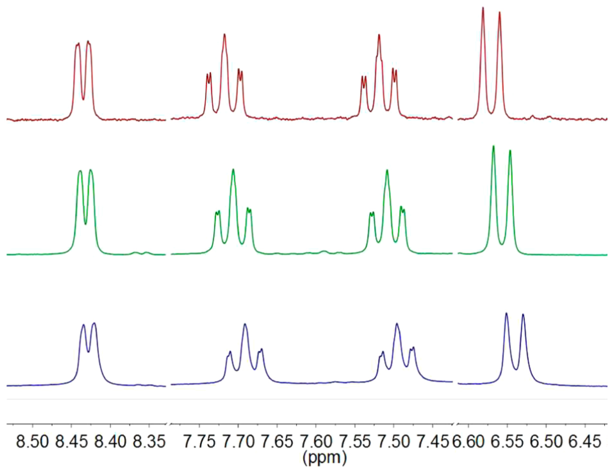

Figure 14. ^{1}H NMR spectra of **3** (top, red), a 1:1 equimolar mixture of **3** and **6** (middle, green), and **6** (bottom, blue) in CD_3CN at room temperature, emphasizing the dpa proton resonances.

Scheme 3. Oxidation of Trialkylphosphines by $[W_2O(dpa)_4]^{2+}$

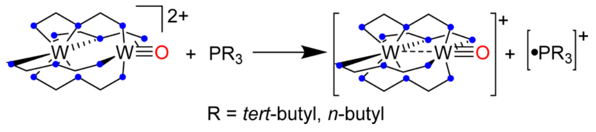

Two aspects of the electronic structure of **7** provide a rationale for this unusual and unexpected metal−oxo reactivity. First, the DFT and CASSCF results indicate a substantially strong W≡O triple bond in **7** (with a W≡O MBO of 2.31 and EBO of 2.85). This strong W≡O bond is therefore rendered inert, similar to the case of other simple mononuclear W(IV)≡O compounds.[32] What makes **7** different from mononuclear W(IV)−oxo compounds is the fact that it can be reduced ($E_{1/2}$ = −1.48 V). Mononuclear W(IV)−oxo compounds are difficult to reduce because the additional electron must be added to the

W−O π* orbitals, which are high in energy (Scheme 4). In **7**, neither of the frontier orbitals is centered on the mononuclear W−O unit; one-electron reduction therefore leads to reduction of the eight-coordinate W^{IV} atom to W^{III}. Interestingly, chemical reduction of **7** using an innocent reducing agent, decamethylcobaltocene, does not lead to an isolable $[W_2O(dpa)_4]^+$ species but instead leads to a mixture of $W_2(dpa)_4$ and unreacted starting material, **7**. We suspect that this over-reduction is due to the formation of a stronger W−W interaction in $[W_2O(dpa)_4]^+$, which renders the oxygen atom labile and leads to facile multielectron reduction to $W_2(dpa)_4$. Similar results were achieved in attempts to reduce **5** with decamethylcobaltocene. The products in this case were $Mo_2(dpa)_4$ and unreacted **5**. These results point to the facile multielectron transfer reactions being mediated by the M···M≡O compounds described here. Future work in our lab will focus on exploring this multielectron reactivity.

Scheme 4. Frontier Orbitals of Mononuclear W(IV)−Oxo and Binuclear W(IV)−Oxo Compounds Associated with One-Electron Reduction

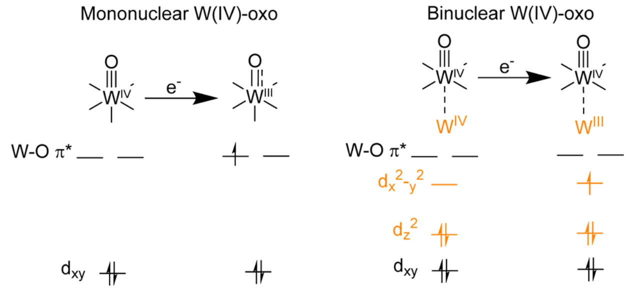

■ CONCLUSIONS

We have presented a case of unusually elastic metal−metal bonds in a systematic series of bimetallic group 6 compounds that facilitate multielectron redox chemistry. Although metal−metal bond scission occurs in the dichromium compound, $Cr_2(dpa)_4$, upon two-electron oxidation, the $Mo_2(dpa)_4$, $MoW(dpa)_4$, and $W_2(dpa)_4$ compounds all experience bond "stretching" without cleavage. The diamagnetic nature of these compounds was confirmed by NMR experiments, and electronic structures calculated using DFT and CASSCF methods provide evidence for an elongated metal−metal triple bond with an unusual $\sigma^2\pi^2\delta^2$ configuration. CASSCF/CASPT2 calculations on $[M_2(dpa)_4]^{2+}$ (M_2 = Mo_2, MoW, W_2) compounds show strong multiconfigurational singlet ground states with a dominant $\sigma^2\pi^2\delta^2$ configuration that becomes more important as the tungsten content increases in the compounds. The preparation and properties of new metal−metal−oxo compounds are also presented. The metal−metal distances in these compounds are outside the single-bond radii of the atoms, and DFT and CASSCF/CASPT2 calculations suggest interactions between the metal centers that are weaker than those in a metal−metal single bond. The presence of an additional metal atom in the coordination sphere of the metal−oxo unit engenders the complexes with enhanced redox capabilities, not unlike the coupling of a metal−oxo to a redox-active heme site in biological systems. Exploration of the implications of this unusual electronic structure for the reactivity is currently underway in our laboratory.

■ EXPERIMENTAL SECTION

Materials and Methods. All of the reactions were carried out under a dry N_2 atmosphere using Schlenk techniques and glovebox methods. Solvents diethyl ether (Et_2O), acetonitrile (CH_3CN), and hexanes were purified using a Vacuum Atmospheres solvent purification system. Dichloromethane was freshly distilled under an N_2 atmosphere over CaH_2 prior to use. Ferrocenium triflate [Fc(OTf)],[33] $Cr_2(dpa)_4$,[4b] $Mo_2(dpa)_4$,[8a] $MoW(dpa)_4$,[4c] and $W_2(dpa)_4$[8a] were prepared according to literature procedures. *m*-CPBA was purchased from Sigma-Aldrich and purified according to literature procedures.[34] Ag(OTf) and tetrabutylammonium tetraphenylborate ($[NBu_4][BPh_4]$) were purchased from Sigma-Aldrich and used as received. Cyclic voltammograms were taken on a BASi potentiostat using Epsilon software in CH_2Cl_2 or CH_3CN solutions with 0.1 M NBu_4PF_6 and 1.0 mM substrate. The electrodes were as follows: glassy carbon (working), Pt wire (auxiliary), and Ag/Ag^+ in CH_3CN (reference). The potentials were referenced versus the ferrocene/ferrocenium (Fc/Fc^+) redox couple using externally added ferrocene. Elemental analysis was carried out by Midwest Microlab, LLC (Indianapolis, IN, USA). The IR spectra were taken on a Bruker TENSOR 27 FTIR spectrometer using an attenuated total reflectance (ATR) adapter. ^1H NMR spectra were recorded on either a Varian INOVA-500 or Bruker AC+ 300 spectrometer. Magnetic susceptibility measurements were obtained using a Quantum Design MPMS-XL SQUID magnetometer. The measurements were performed on a polycrystalline sample of **1** (7.8 mg) introduced in a polyethylene bag (3 cm × 0.5 cm × 0.02 cm). The direct-current (dc) measurements were conducted from 340 to 1.8 K at an applied dc field of 1000 Oe. An *M* versus *H* measurement was performed at 100 K to confirm the absence of ferromagnetic impurities. The EPR measurement was carried out at room temperature on a 1 mM CH_2Cl_2 solution using a Bruker EleXsys EPR spectrometer (E-500-A console with ER 049SX SuperX bridge and SuperX cavity). The parameters were as follows: microwave frequency = 9.8459 GHz, microwave power = 2 mW, field center = 3700 G, field width = 600 G, modulation amplitude = 4 G, modulation frequency = 100 kHz, time constant = 163.84 ms.

X-ray Structure Determinations. Crystallographic data were measured at the Molecular Structure Laboratory of the Chemistry Department of the University of Wisconsin-Madison. Crystals were selected under oil under ambient conditions and attached to the tip of a MiTeGen MicroMount. Each crystal was mounted in a stream of cold nitrogen at 100(1) K and centered in the X-ray beam using a video camera. The crystal evaluation and data collection were performed on a Bruker Quazar SMART APEX II diffractometer with Mo Kα (λ = 0.71073 Å) or Cu Kα (λ = 1.54178 Å) radiation at a detector to crystal distance of 4.96 or 4.03 cm, respectively. The data were collected using a routine to survey an entire sphere of reciprocal space and were indexed using the SMART program.[35] The structures were solved using direct methods and refined by least-squares refinement on F^2 followed by difference Fourier synthesis.[36] All of the hydrogen atoms were included in the final structure factor calculation at idealized positions and were allowed to ride on the neighboring atoms with relative isotropic displacement coefficients.

Computational Methods. The initial coordinates of **1**−**7** were obtained from the crystallographic data for the compounds with the solvent molecules of crystallization removed. All of the geometry optimizations were carried out with ORCA version 2.9.1[37] and the BP86 exchange−correlation functional.[38] The B3LYP functional[39] was used for the broken-symmetry calculations on **1**. The def2-TZVPP basis set[40] including all-electron scalar relativistic effects within the ZORA approximation[41] was used with the def2-TZVPP/J auxiliary basis set for N, Mo, and W. The def2-SVP basis set[42] with the def2-SVP/J auxiliary basis set was used for all of the remaining atoms. Tight optimization and tight self-consistent field convergence criteria were employed along with grid5 for all calculations. Frequency calculations were performed following geometry optimizations to ensure minimum-energy structures.

CASSCF/CASPT2 calculations were performed using the MOLCAS 7.7 package.[43] Basis sets of the atomic natural orbital type with triple-ζ plus polarization quality (ANO-RCC-VTZP) for the molybdenum, tungsten, and oxygen atoms and with double-ζ plus polarization quality for the nitrogen and carbon atoms (ANO-RCC-VDZP) were used, whereas a minimal basis set (ANO-RCC-MB) was used for the hydrogen atoms. Scalar relativistic effects were included using the Douglas−Kroll−Hess Hamiltonian. The computational costs arising from the two-electron integrals were drastically reduced by employing the Cholesky decomposition technique.[44] The decomposition threshold was chosen to be 10^{-4}. The crystal structure coordinates were used for all compounds analyzed. No symmetry constraints were used in the calculations. At the CASPT2 level of theory, in order to prevent weak intruder states, an imaginary shift of 0.2 units was added to the external part of the zeroth-order Hamiltonian. For all of the compounds, carbon and nitrogen 1s orbitals were kept frozen. For $[Mo_2(dpa)_4]^{2+}$ and $[Mo_2O(dpa)_4]^{2+}$, orbitals up to and including the 3d orbitals for the Mo atoms were kept frozen. For $[MoW(dpa)_4]^{2+}$ and $[WMoO(dpa)_4]^{2+}$, orbitals up to and including the 3d orbitals for the Mo atom and the 4d orbitals for the W atom were kept frozen. For $[W_2(dpa)_4]^{2+}$ and $[W_2O(dpa)_4]^{2+}$, orbitals up to and including the 4d orbitals for the W atoms were kept frozen. In order to further reduce the computational cost, the 300 highest-energy secondary orbitals were deleted at the CASPT2 level. The standard 0.25 IPEA value was used for the zeroth-order Hamiltonian operator. For the $[M_2(dpa)_4]^{2+}$ compounds, the active space included six active electrons (three per metal center) distributed in six orbitals (three per metal center) [denoted as CAS(6,6)]. For the $[M_2O(dpa)_4]^{2+}$ compounds, the active space included 10 electrons (six from oxygen and two from each metal center) distributed in eight orbitals (the bonding and antibonding combinations of the metal−oxygen σ and π orbitals, the d_{z^2} orbital of the eight-coordinate metal atom, and the d_{xy} orbital of the metal atom bound to oxygen) [denoted as CAS(10,8)]. CASSCF and CASPT2 calculations were performed for the lowest singlet, triplet, quintet, and septet spin states for **1**−**4** and the lowest singlet and triplet spin states for **5**−**7**.

Syntheses. *$[Cr_2(dpa)_4](OTf)_2$ (**1**).* A slurry of Ag(OTf) (0.22 g, 0.86 mmol) in CH_2Cl_2 (8 mL) was added to a solution of $Cr_2(dpa)_4$ (0.30 g, 0.38 mmol) in CH_2Cl_2 (20 mL), resulting in an instant color change from orange to red-brown. After 15 min of stirring, the mixture turned brown. After 1 h, the reaction mixture was filtered, and the brown filtrate was layered with hexanes (50 mL). Small red needle crystals suitable for X-ray diffraction formed overnight. Yield: 0.18 g (43%). Anal. Calcd for $C_{42}H_{32}Cr_2F_6N_{12}O_6S_2$: C 46.58%, H 2.98%, N 15.52%. Found: C 46.48%, H 2.98%, N 15.52%. ^1H NMR (CD_2Cl_2, 500 MHz, ppm): δ −5.18 (3H, br), 1.56 (1H, br), 3.94 (1H, br), 12.83 (1H, br). IR (KBr, cm^{-1}): 1607 s, 1595 s, 1563 w, 1557 w, 1486 s, 1470 s, 1443 s, 1381 m, 1316 m, 1256 s, 1155 s, 1032 s, 831 w, 768 s, 736 w, 662 w, 635 s.

*$[Mo_2(dpa)_4](OTf)_2$ (**2**).* A blue solution of Fc(OTf) (0.40 g, 1.2 mmol) in CH_2Cl_2 (35 mL) was slowly added at room temperature to a stirred slurry of $Mo_2(dpa)_4$ (0.48 g, 0.55 mmol) in CH_2Cl_2 (15 mL). An immediate color change from red to green-brown and then to red-brown upon further addition was observed. After the mixture was stirred for 30 min, Et_2O (60 mL) was added, resulting in the formation of a brown precipitate, which was isolated by filtration, quickly washed with CH_2Cl_2 (20 mL), and dried under reduced pressure. Yield: 0.48 g (75%). Crystals of **2** were obtained by dissolving the precipitate in CH_3CN followed by solvent diffusion of Et_2O inside a reaction flask. Anal. Calcd for $C_{42}H_{32}F_6Mo_2N_{12}O_6S_2\cdot CH_2Cl_2$:[45] C 41.13%, H 2.73%, N 13.39%. Found: C 41.55%, H 2.84%, N, 13.11%. ^1H NMR (CD_3CN, 500 MHz, ppm): δ 8.09 (4H, d, J = 8.9 Hz), 7.65 (4H, s), 7.40 (4H, d, J = 8.1 Hz), 7.05 (4H, t, J = 6.8 Hz), 6.97 (4H, s), 6.88 (4H, t, J = 7.7 Hz), 6.67 (4H, t, J = 8.1 Hz), 6.44 (4H, s). IR (ATR, cm^{-1}): 1605 m, 1591 m, 1482 m, 1465 s, 1443 m, 1384 w, 1317 w, 1254 s, 1164 m, 1150 m, 1029 m, 926 w, 835 w, 765 s, 734 w, 634 s.

*$[MoW(dpa)_4](OTf)_2$ (**3**).* A slurry of $MoW(dpa)_4$ (0.34 g, 0.35 mmol) in CH_2Cl_2 (30 mL) was added to a slurry of Ag(OTf) (0.19 g, 0.73 mmol) in CH_2Cl_2 (10 mL). After 3 h of stirring, the resulting green-black mixture was filtered and layered with hexanes (60 mL), yielding black plate-like crystals suitable for X-ray diffraction. Yield: 0.21 g (47%). Anal. Calcd for $C_{42}H_{32}F_6MoN_{12}O_6S_2W\cdot CH_2Cl_2$:[45] C 38.44%, H 2.55%, N 12.51%. Found: C 38.81%, H 2.63%, N 12.22%. ^1H NMR (CD_3CN, 400 MHz, ppm): δ 8.54 (4H, d, J = 5.8 Hz), 7.75 (4H, t, J = 8.7 Hz), 7.75 (4H, t, J = 8.6 Hz), 7.37 (4H, d, J = 4.9 Hz), 6.97−6.89 (8H, m), 6.80 (4H, d, J = 8.4 Hz), 6.59 (4H, d, J = 8.6 Hz). IR (ATR, cm^{-1}): 1605 m, 1463 s, 1441 m, 1383 w, 1256 m, 1223 w, 1151 m, 1029 m, 909 w, 839 w, 764 m, 740 w, 635 s.

*$[W_2(dpa)_4](OTf)_2$ (**4**).* A blue solution of Fc(OTf) (0.34 g, 1.0 mmol) in CH_2Cl_2 (35 mL) was added at room temperature to a stirred slurry of $W_2(dpa)_4$ (0.50 g, 0.48 mmol) in CH_2Cl_2 (10 mL) over the course of 5 min. An immediate color change from purple to violet and then to brown upon further addition was observed with concomitant formation of a precipitate. After the mixture was stirred for 30 min, Et_2O (60 mL) was added, resulting in the formation of more precipitate, which was isolated by filtration, quickly washed with CH_2Cl_2 (20 mL), and dried under reduced pressure. Yield: 0.51 g (79%). Crystals of **3** were obtained by dissolving the precipitate in CH_3CN followed by fast solvent diffusion of Et_2O inside a reaction flask. Anal. Calcd for $C_{42}H_{32}F_6N_{12}O_6S_2W_2$: C 37.46%, H 2.40%, N 12.48%. Found: C 37.69%, H 2.66%, N 12.18%. ^1H NMR (CD_3CN, 300 MHz, ppm): δ 8.62 (4H, d, J = 5.3 Hz), 7.93 (4H, t, J = 7.6 Hz), 7.66 (4H, d, J = 8.9 Hz), 7.53 (4H, d, J = 6.0 Hz), 7.31 (4H, d, J = 8.7 Hz), 7.28−7.23 (4H, t, J = 6.6 Hz), 7.18 (4H, t, J = 7.4 Hz), 6.55 (4H, t, J = 6.2 Hz). IR (KBr, cm^{-1}): 1708 w, 1654 w, 1606 m, 1590 m, 1479 m, 1461 s, 1442 s, 1319 w, 1262 s, 1236 m, 1222 w, 1149 m, 1030 m, 830 w, 764 m, 734 w, 636 m.

*$[Mo_2O(dpa)_4](OTf)(BPh_4)$ (**5**).* A solution of *m*-CPBA (0.05 g, 0.3 mmol) in CH_2Cl_2 (10 mL) was added to a stirred solution of **2** (0.29 g, 0.24 mmol) in CH_2Cl_2 (25 mL), resulting in a color change from brown to red-brown. After 3 h of stirring, a solution of NBu_4BPh_4 (0.15 g, 0.27 mmol) in CH_3CN (10 mL) was added, and the mixture was stirred for an additional 30 min. The reaction mixture was then filtered and layered with hexanes (60 mL) to yield crystalline **5**. Recrystallization from CH_3CN and Et_2O yielded brown block crystals suitable for X-ray diffraction. Yield: 0.09 g (30%). Anal. Calcd for $C_{71}H_{65}BF_3Mo_2N_{13}O_5S$: C 57.93%, H 4.45%, N 12.37%. Found: C 58.36%, H 4.57%, N 12.48%. ^1H NMR (CD_3CN, 400 MHz, ppm): δ 8.45 (4H, d, J = 5.2 Hz), 7.67 (4H, t, J = 8.1 Hz), 7.52 (4H, t, J = 7.5 Hz), 7.25 (12H, m), 7.01 (16H, m), 6.85 (8H, d, J = 8.4 Hz), 6.63 (4H, d, J = 8.5 Hz). IR (ATR, cm^{-1}): 1602 m, 1592 m, 1463 s, 1436 m, 1373 w, 1279 m, 1257 m, 1152 m, 1030 m, 973 w, 908 w, 833 w, 764 s, 741 m, 731 s, 704 s, 668 w, 648 w, 637 s, 625 w, 606 m.

*$[WMoO(dpa)_4](OTf)(BPh_4)$ (**6**).* A solution of *m*-CPBA (0.03 g, 0.2 mmol) in CH_2Cl_2 (10 mL) was added to a stirred solution of **3** (0.12 g, 0.095 mmol) in CH_2Cl_2 (30 mL), resulting in a color change from brown to green-black. After 3 h of stirring, a solution of NBu_4BPh_4 (0.06 g, 0.1 mmol) in CH_2Cl_2 (10 mL) was added, and the mixture was stirred for an additional 30 min. The reaction mixture was filtered and layered with hexanes (60 mL) to yield crystalline **6**. Recrystallization from CH_3CN and Et_2O yielded brown block crystals suitable for X-ray diffraction. Yield: 0.06 g (40%). Anal. Calcd for $C_{71}H_{65}BF_3MoN_{13}O_5SW$: C 54.66%, H 4.20%, N 11.67%. Found: C 54.51%, H 4.33%, N 11.32%. ^1H NMR (CD_3CN, 400 MHz, ppm): δ 8.43 (4H, d, J = 5.8 Hz), 7.69 (4H, t, J = 7.6 Hz), 7.50 (4H, t, J = 7.2 Hz), 7.35 (4H, d, J = 5.6 Hz), 7.26 (8H, s), 6.99−6.87 (16H, m), 6.83 (4H, t, J = 7.2 Hz), 6.76 (4H, d, J = 8.4 Hz), 6.54 (4H, d, J = 8.5 Hz). IR (ATR, cm^{-1}): 1604 w, 1463 s, 1437 w, 1382 w, 1258 s, 1152 m, 1093 m, 1029 s, 955 w, 798 s, 764 s, 742 m, 731 m, 704 s, 637 s, 614 w, 606 m.

*$[W_2O(dpa)_4](OTf)(BPh_4)$ (**7**).* A solution of *m*-CPBA (0.092 g, 0.53 mmol) in CH_3CN (10 mL) was added to a stirred solution of **4** (0.51 g, 0.38 mmol) in CH_3CN, resulting in an immediate color change from yellow-brown to green-brown. The mixture was stirred for 3 h, and the brown solution was filtered into a flask containing dried NBu_4BPh_4 (0.43 g, 0.77 mmol). Solvent diffusion of Et_2O (100 mL) into this solution yielded crystalline **7**. Crystalline yield: 0.24 g, (38%). Anal. Calcd for $C_{71}H_{65}BF_3N_{13}O_5SW_2$: C 51.75%, H 3.98%, N 11.05%. Found: C 51.71%, H 4.08%, N 10.78%. ^1H NMR (CD_3CN, 300 MHz, ppm): δ 8.29 (4H, ddd, J = 5.8, 1.7, 0.8 Hz), 7.72 (4H, ddd, J = 8.6, 7.6, 1.7 Hz), 7.45 (4H, ddd, J = 5.6, 1.6, 0.9 Hz), 7.30−7.27 (8H, m, *o*-1H of $B(C_6H_5)_4$), 7.12 (4H, ddd, J = 8.4, 7.3, 1.7 Hz), 7.03−6.95

(16H, m), 6.87−6.84 (8H, m), 6.63 (4H, dt, J = 8.6, 0.9 Hz). ^{19}F NMR (CD_3CN, 282 MHz, ppm): δ −83.83 (s). IR (KBr, cm^{-1}): 1716 w, 1701 w, 1603 m, 1594 m, 1463 s, 1436 m, 1313 w, 1279 w, 1258 m, 1223 m, 1152 w, 1119 m, 1031 w, 957 w, 839 w, 764 w, 742 w, 733 w, 706 w, 613 w.

[MoW(dpa)$_4$](OTf) (8). A slurry of MoW(dpa)$_4$ (0.18 g, 0.19 mmol) in CH_2Cl_2 (20 mL) was added to a slurry of Ag(OTf) (0.05 g, 0.2 mmol) in CH_2Cl_2 (10 mL). After 3 h of stirring, the green-black solution was filtered and layered with hexanes (60 mL) to yield black plate crystals suitable for X-ray diffraction. Yield: 0.06 g (30%). Anal. Calcd for $C_{41}H_{32}F_3MoN_{12}O_3SW\cdot CH_2Cl_2$:[45] C 42.23%, H 2.87%, N 14.07%. Found: C 42.54%, H 3.01%, N 14.06%. IR (ATR, cm^{-1}): 1600 m, 1583 m, 1457 s, 1432 s, 1305 w, 1261 s, 1223 w, 1152 m, 1029 m, 910 w, 835 w, 735 s, 695 m, 668 w, 645 s, 636 m.

■ ASSOCIATED CONTENT

Ⓢ Supporting Information

Additional figures as noted in the text, Cartesian coordinates for all of the optimized structures, and crystallographic data (CIF). This material is available free of charge via the Internet at http://pubs.acs.org.

■ AUTHOR INFORMATION

Corresponding Author

*E-mail: berry@chem.wisc.edu.

Notes

The authors declare no competing financial interest.

■ ACKNOWLEDGMENTS

J.F.B. thanks the National Science Foundation for support under Grant CHE-1300464. DFT calculations performed at the University of Wisconsin were done using infrastructure supported by the National Science Foundation under Grant CHE-0840494. NMR data were acquired on instruments supported by the National Science Foundation under Grant CHE-1048642 and a generous gift from Paul J. Bender. The multiconfigurational computations (G.L.M. and L.G.) are based on work supported by the National Science Foundation under Grant CHE-1212575. E.A.H. and R.C. acknowledge CNRS, Université Bordeaux, Région Aquitaine, and ANR for financial support and M. Rouzières for SQUID sample preparation and technical help during the magnetic measurements.

■ REFERENCES

(1) Nguyen, T.; Sutton, A. D.; Brynda, M.; Fettinger, J. C.; Long, G. J.; Power, P. P. *Science* **2005**, *310*, 844−847.

(2) (a) Wagner, F. R.; Noor, A.; Kempe, R. *Nat. Chem.* **2009**, *1*, 529−536. (b) Horvath, S.; Gorelsky, S. I.; Gambarotta, S.; Korobkov, I. *Angew. Chem., Int. Ed.* **2008**, *47*, 9937−9940. (c) Kreisel, K. A.; Yap, G. P. A.; Dmitrenko, O.; Landis, C. R.; Theopold, K. H. *J. Am. Chem. Soc.* **2007**, *129*, 14162−14163. (d) Hsu, C.-W.; Yu, J.-S. K.; Yen, C.-H.; Lee, G.-H.; Wang, Y.; Tsai, Y.-C. *Angew. Chem., Int. Ed.* **2008**, *47*, 9933−9936. (e) Tsai, Y.-C.; Hsu, C.-W.; Yu, J.-S. K.; Lee, G.-H.; Wang, Y.; Kuo, T.-S. *Angew. Chem., Int. Ed.* **2008**, *47*, 7250−7253. (f) Noor, A.; Wagner, F. R.; Kempe, R. *Angew. Chem., Int. Ed.* **2008**, *47*, 7246−7249. (g) Tsai, Y.-C.; Chen, H.-Z.; Chang, C.-C.; Yu, J.-S. K.; Lee, G.-H.; Wang, Y.; Kuo, T.-S. *J. Am. Chem. Soc.* **2009**, *131*, 12534−12535. (h) La Macchia, G.; Li Manni, G.; Todorova, T. K.; Brynda, M.; Aquilante, F.; Roos, B. O.; Gagliardi, L. *Inorg. Chem.* **2010**, *49*, 5216−5222. (i) Liu, S.-C.; Ke, W.-L.; Yu, J.-S. K.; Kuo, T.-S.; Tsai, Y.-C. *Angew. Chem., Int. Ed.* **2012**, *51*, 6394−6397. (j) Harisomayajula, N. V. S.; Nair, A. K.; Tsai, Y.-C. *Chem. Commun.* **2014**, *50*, 3391−3412. (k) Hoa, S.-A.; Tsai, Y.-C.; Peng, S.-M. *J. Chin. Chem. Soc.* **2014**, *61*, 9−26 and references therein.

(3) (a) Harris, T. D.; Zhao, Q.; Sanchez, R. H.; Betley, T. A. *Chem. Commun.* **2011**, *47*, 6344−6346. (b) Zhao, Q.; Betley, T. A. *Angew. Chem., Int. Ed.* **2011**, *50*, 709−712. (c) Zhao, Q.; Harris, T. D.; Betley, T. A. *J. Am. Chem. Soc.* **2011**, *133*, 8293−8306.

(4) (a) Berry, J. F. *Struct. Bonding* **2010**, *136*, 1−28. (b) Nippe, M.; Berry, J. F. *J. Am. Chem. Soc.* **2007**, *129*, 12684−12685. (c) Nippe, M.; Timmer, G. H.; Berry, J. F. *Chem. Commun.* **2009**, 4357−4359. (d) Nippe, M.; Victor, E.; Berry, J. F. *Eur. J. Inorg. Chem.* **2008**, 5569−5572. (e) Nippe, M.; Wang, J.; Bill, E.; Hope, H.; Dalal, N. S.; Berry, J. F. *J. Am. Chem. Soc.* **2010**, *132*, 14261−14272. (f) Nippe, M.; Bill, E.; Berry, J. F. *Inorg. Chem.* **2011**, *50*, 7650−7661. (g) Nippe, M.; Turov, Y.; Berry, J. F. *Inorg. Chem.* **2011**, *50*, 10592−10599. (h) Turov, Y.; Berry, J. F. *Dalton Trans.* **2012**, *41*, 8153−8161. (i) Aydin-Cantürk, D.; Nuss, H. *Z. Anorg. Allg. Chem.* **2011**, *637*, 543−546. (j) Huang, G.-C.; Bénard, M.; Rohmer, M.-M.; Li, L.-A.; Chiu, M.-J.; Yeh, C.-Y.; Lee, G.-H.; Peng, S.-M. *Eur. J. Inorg. Chem.* **2008**, 1767−1777. (k) Rohmer, M.-M.; Liu, I. P.-C.; Lin, J.-C.; Chiu, M.-J.; Lee, C.-H.; Lee, G.-H.; Bénard, M.; López, X.; Peng, S.-M. *Angew. Chem., Int. Ed.* **2007**, *46*, 3533−3536. (l) Thomas, C. M. *Comments Inorg. Chem.* **2011**, *32*, 14−38. (m) Greenwood, B. P.; Forman, S. I.; Rowe, G. T.; Chen, C.-H.; Foxman, B. M.; Thomas, C. M. *Inorg. Chem.* **2009**, *48*, 6251−6260. (n) Greenwood, B. P.; Rowe, G. T.; Chen, C.-H.; Foxman, B. M.; Thomas, C. M. *J. Am. Chem. Soc.* **2010**, *132*, 44−45. (o) Evers, D. A.; Bluestein, A. H.; Foxman, B. M.; Thomas, C. M. *Dalton Trans.* **2012**, *41*, 8111−8115. (p) Lin, T.-P.; Wade, C. R.; Pérez, L. M.; Gabbaï, F. P. *Angew. Chem.* **2010**, *122*, 6501−6504. (q) Lin, T.-P.; Ke, I.-S.; Gabbaï, F. P. *Angew. Chem., Int. Ed.* **2012**, *51*, 4985−4988. (r) Lin, T.-P.; Nelson, R. C.; Wu, T.; Miller, J. T.; Gabbaï, F. P. *Chem. Sci.* **2012**, *3*, 1128−1136. (s) Cheng, M.-C.; Mai, C.-L.; Yeh, C.-Y.; Lee, G.-H.; Peng, S.-M. *Chem. Commun.* **2013**, *49*, 7938−7940. (t) Rudd, P. A.; Liu, S.; Planas, N.; Bill, E.; Gagliardi, L.; Lu, C. C. *Angew. Chem., Int. Ed.* **2013**, *52*, 4449−4452. (u) Zall, C. M.; Clouston, L. J.; Young, V. G.; Ding, K.; Kim, H. J.; Zherebetskyy, D.; Chen, Y.-S.; Bill, E.; Gagliardi, L.; Lu, C. C. *Inorg. Chem.* **2013**, *52*, 9216−9228. (v) Clouston, L. J.; Siedschlag, R. B.; Rudd, P. A.; Planas, N.; Hu, S.; Miller, A. D.; Gagliardi, L.; Lu, C. C. *J. Am. Chem. Soc.* **2013**, *135*, 13142−13148. (w) Dolinar, B. S.; Berry, J. F. *Inorg. Chem.* **2013**, *52*, 4658−4667.

(5) (a) Gagliardi, L.; Roos, B. O. *Nature* **2005**, *433*, 848−851. (b) Roos, B. O.; Gagliardi, L. *Inorg. Chem.* **2006**, *45*, 803−807. (c) Wu, X.; Lu, X. *J. Am. Chem. Soc.* **2007**, *129*, 2171−2177. (d) Arnold, P. L.; Jones, G. M.; Odoh, S. O.; Schreckenbach, G.; Magnani, N.; Love, J. B. *Nat. Chem.* **2012**, *4*, 221−227.

(6) Cotton, F. A.; Murillo, C. A.; Walton, R. A. *Multiple Bonds between Metal Atoms*, 3rd ed.; Springer Science and Business Media: New York, 2005; p 817.

(7) (a) Cotton, F. A.; Murillo, C. A.; Zhou, H.-C. *Inorg. Chem.* **2000**, *39*, 3261−3264. (b) Carlson-Day, K. M.; Eglin, J. L.; Lin, C.; Smith, L. T.; Staples, R. J.; Wipf, D. O. *Polyhedron* **1999**, *18*, 817−824. (c) Chisholm, M. H. *Coord. Chem. Rev.* **2013**, *257*, 1576−1583. (d) Cotton, F. A.; Feng, X.; Matusz, M. *Inorg. Chem.* **1989**, *28*, 594−601. (e) Cotton, F. A.; Daniels, L. M.; Huang, P.; Murillo, C. A. *Inorg. Chem.* **2001**, *41*, 317−320. (f) Cotton, F. A.; Dalal, N. S.; Hillard, E. A.; Huang, P.; Murillo, C. A.; Ramsey, C. M. *Inorg. Chem.* **2003**, *42*, 1388−1390. (g) Bailey, P. J.; Bone, S. F.; Mitchell, L. A.; Parsons, S.; Taylor, K. J.; Yellowlees, L. J. *Inorg. Chem.* **1997**, *36*, 867−871. (h) Bailey, P. J.; Bone, S. F.; Mitchell, L. A.; Parsons, S.; Taylor, K. J.; Yellowlees, L. J. *Inorg. Chem.* **1997**, *36*, 5420. (i) Cotton, F. A.; Daniels, L. M.; Hillard, E. A.; Murillo, C. A. *Inorg. Chem.* **2002**, *41*, 1639−1644. (j) Chisholm, M. H.; D'Acchioli, J. S.; Pate, B. D.; Patmore, N. J.; Dalal, N. S.; Zipse, D. J. *Inorg. Chem.* **2005**, *44*, 1061−1067. (k) Chisholm, M. H.; Patmore, N. J. *Can. J. Chem.* **2009**, *87*, 88−94. (l) Cotton, F. A.; Murillo, C. A.; Wang, X.; Wilkinson, C. C. *Dalton Trans.* **2006**, 4623−4631. (m) Cotton, F. A.; Huang, P.; Murillo, C. A.; Timmons, D. J. *Inorg. Chem. Commun.* **2002**, *5*, 501−504. (n) Cotton, F. A.; Daniels, L. M.; Murillo, C. A.; Timmons, D. J.; Wilkinson, C. C. *J. Am. Chem. Soc.* **2002**, *124*, 9249−9256. (o) Cotton, F. A.; Huang, P.; Murillo, C. A.; Wang, X. *Inorg. Chem. Commun.* **2003**, *6*, 121−126. (p) Chisholm, M. H.; Gallucci, J.; Hadad, C. M.; Huffman, J. C.; Wilson, P. J. *J. Am. Chem. Soc.* **2003**, *125*, 16040−16049.

(8) (a) Nippe, M.; Victor, E.; Berry, J. F. *Inorg. Chem.* **2009**, *48*, 11889−11895. (b) Cotton, F. A.; Daniels, L. M.; Murillo, C. A.; Timmons, D. J. *Chem. Commun.* **1997**, 1449−1450.

(9) Bino, A.; Cotton, F. A. *Angew. Chem., Int. Ed. Engl.* **1979**, *18*, 462−463.

(10) Clérac, R.; Cotton, F. A.; Jeffery, S. P.; Murillo, C. A.; Wang, X. *Dalton Trans.* **2003**, 3022−3027.

(11) (a) Wilson, L. M.; Cannon, R. D. *Inorg. Chem.* **1988**, *27*, 2382−2383. (b) Alfaro, N. M.; Cotton, F. A.; Daniels, L. M.; Murillo, C. A. *Inorg. Chem.* **1992**, *31*, 2718−2723. (c) Sadique, A. R.; Heeg, M. J.; Winter, C. H. *J. Am. Chem. Soc.* **2003**, *125*, 7774−7775. (d) El-Kadri, O. M.; Heeg, M. J.; Winter, C. H. *Inorg. Chem.* **2006**, *45*, 5278−5280.

(12) (a) Hall, M. B. *Polyhedron* **1987**, *6*, 679−684. (b) Andersson, K.; Bauschlicher, C. W., Jr.; Persson, B. J.; Roos, B. O. *Chem. Phys. Lett.* **1996**, *257*, 238−248. (c) Li Manni, G.; Dzubak, A. L.; Mulla, A.; Brogden, D. W.; Berry, J. F.; Gagliardi, L. *Chem.—Eur. J.* **2012**, *18*, 1737−1749.

(13) Similar Ru−Ru≡O species have been proposed as intermediates in catalysis. See: Villalobos, L.; Barker Paredes, J. E.; Cao, Z.; Ren, T. *Inorg. Chem.* **2013**, *52*, 12545−12552.

(14) The increased solubility of **3** in dichloromethane can be attributed to its dipole moment, which was calculated (by DFT) to be 0.7 D; in contrast, the dipole moments of **2** and **4** are negligible.

(15) Nippe, M.; Goodman, S. M.; Fry, C. G.; Berry, J. F. *J. Am. Chem. Soc.* **2011**, *133*, 2856−2859.

(16) Refinements of **6** without metal atom disorder resulted in non-positive-definite atoms.

(17) Cotton, F. A.; Daniels, L. M.; Murillo, C. A.; Pascual, I.; Zhou, H.-C. *J. Am. Chem. Soc.* **1999**, *121*, 6856−6861.

(18) The sample studied was shown by crystallography to contain >85% W···Mo≡O isomer.

(19) (a) Theopold, K. H. *Acc. Chem. Res.* **1990**, *23*, 263−270. (b) Clérac, R.; Cotton, F. A.; Murillo, C. A.; Wang, X. *Chem. Commun.* **2001**, 205−206.

(20) There is a minor contribution from a $[Mo_2(dpa)_4]^+$ impurity with g_{iso} = 1.951 and A_{iso} = 56 MHz, which values are identical to those previously reported for $[Mo_2(dpa)_4]^+$.

(21) We note that the sample of **6** analyzed by ^{1}H NMR spectroscopy was shown by X-ray crystallography to contain ca. 90% W···Mo≡O isomer. Thus, only one set of signals was observed. However, we cannot rule out the possibility that both isomers are present but interconvert too rapidly to be observed on the NMR time scale.

(22) Pyykkö, P.; Atsumi, M. *Chem.—Eur. J.* **2009**, *15*, 186−197.

(23) Alvarez, S. *Dalton Trans.* **2013**, *42*, 8617−8636.

(24) For **6**, the lower-energy isomer, Mo···W≡O, was chosen for this comparison.

(25) Berry, J. F.; Bothe, E.; Cotton, F. A.; Ibragimov, S. A.; Murillo, C. A.; Villagrán, D.; Wang, X. *Inorg. Chem.* **2006**, *45*, 4396−4406.

(26) Cotton, F. A.; Diebold, M. P.; O'Connor, C.; Powell, G. L. *J. Am. Chem. Soc.* **1985**, *107*, 7438−7445.

(27) (a) McGrady, J. E.; Stranger, R.; Lovell, T. *Inorg. Chem.* **1998**, *37*, 3802−3808. (b) Shaik, S.; Hoffmann, R.; Fisel, C. R.; Summerville, R. H. *J. Am. Chem. Soc.* **1980**, *102*, 4555−4572. (c) Stranger, R.; Lovell, T.; McGrady, J. E. *Inorg. Chem.* **1999**, *38*, 5510−5518. (d) Cavigliasso, G.; Yu, C.-Y.; Stranger, R. *Polyhedron* **2007**, *26*, 2942−2948.

(28) (a) Noodleman, L.; Norman, J. G. *J. Chem. Phys.* **1979**, *70*, 4903−4906. (b) Noodleman, L. *J. Chem. Phys.* **1981**, *74*, 5737−5743.

(29) (a) Yamaguchi, K.; Takahara, Y.; Fueno, T. Ab Initio Molecular Orbital Studies of Structure and Reactivity of Transition Metal−Oxo Compounds. In *Applied Quantum Chemistry*; Smith, V., Jr., Schaefer, H. F., III, Morokuma, K., Eds.; Springer: Dordrecht, The Netherlands, 1986; pp 155−184. (b) Soda, T.; Kitagawa, Y.; Onishi, T.; Takano, Y.; Shigeta, Y.; Nagao, H.; Yoshioka, Y.; Yamaguchi, K. *Chem. Phys. Lett.* **2000**, *319*, 223−230.

(30) Ballhausen, C. J.; Gray, H. B. *Inorg. Chem.* **1962**, *1*, 111−122.

(31) (a) Weinhold, F.; Landis, C. R. *Valency and Bonding*; Cambridge University Press: Cambridge, U.K., 2005. (b) Berry, J. F. *Dalton Trans.* **2012**, *41*, 700−713.

(32) Holm, R. H. *Chem. Rev.* **1987**, *87*, 1401−1449.

(33) Bailey, B. C.; Basuli, F.; Huffman, J. C.; Mindiola, D. J. *Organometallics* **2006**, *25*, 2725−2728.

(34) Davies, D. M.; Jones, P.; Mantle, D. *Biochem. J.* **1976**, *157*, 247−253.

(35) *APEX2, SADABS, and SAINT Software Reference Manuals*; Bruker-AXS: Madison, WI, 2009.

(36) Dolomanov, O. V.; Bourhis, L. J.; Gildea, R. J.; Howard, J. A. K.; Puschmann, H. *J. Appl. Crystallogr.* **2009**, *42*, 339−341.

(37) Neese, F. *ORCA: An ab Initio Density Functional and Semiempirical Program Package*; University of Bonn: Bonn, Germany, 2006.

(38) (a) Becke, A. D. *Phys. Rev. A* **1988**, *38*, 3098−3100. (b) Perdew, J. P. *Phys. Lett. A* **1992**, *165*, 79−82.

(39) (a) Kim, K.; Jordan, K. D. *J. Phys. Chem.* **1994**, *98*, 10089−10094. (b) Stephens, P. J.; Devlin, F. J.; Chabalowski, C. F.; Frisch, M. J. *J. Phys. Chem.* **1994**, *98*, 11623−11627. (c) Becke, A. D. *J. Chem. Phys.* **1993**, *98*, 5648−5652. (d) Lee, C.; Yang, W.; Parr, R. G. *Phys. Rev. B* **1988**, *37*, 785−789.

(40) Schäfer, A.; Huber, C.; Ahlrichs, R. *J. Chem. Phys.* **1994**, *100*, 5829−5835.

(41) van Wüllen, C. *J. Chem. Phys.* **1998**, *109*, 392−399.

(42) Schäfer, A.; Horn, H.; Ahlrichs, R. *J. Chem. Phys.* **1992**, *97*, 2571−2577.

(43) Karlström, G.; Lindh, R.; Malmqvist, P.-Å.; Roos, B. O.; Ryde, U.; Veryazov, V.; Widmark, P.-O.; Cossi, M.; Schimmelpfennig, B.; Neogrady, P.; Seijo, L. *Comput. Mater. Sci.* **2003**, *28*, 222−239.

(44) (a) Aquilante, F.; Malmqvist, P.-Å.; Pedersen, T. B.; Ghosh, A.; Roos, B. O. *J. Chem. Theory Comput.* **2008**, *4*, 694−702. (b) Aquilante, F.; Pedersen, T. B.; Lindh, R.; Roos, B. O.; de Meras, A. S.; Koch, H. *J. Chem. Phys.* **2008**, *129*, No. 024113.

(45) Although dichloromethane was not present in the crystal lattice of the samples used for X-ray crystallographic analysis, the microcrystalline samples sent for elemental analysis were found to contain 1 molar equiv of dichloromethane solvate.